universität wien

ENDBERICHT / FINAL REPORT

Titel des Endberichts / Title of the final report

Live two-color time-lapse STED imaging of the ER and associated proteins in mitotic mammalian cells

verfasst von / submitted by

Sarah Schweighofer, BSc.

Wien, 2016 / Vienna 2016

Betreut von / Supervisor: Dr. Graham Warren

Mitbetreut von / Co-Supervisor: Dr. Joerg Bewersdorf

Acknowledgments

Yale

The official supervisor of my thesis for the University of Vienna was Dr. Graham Warren. The practical work for my thesis was performed in the group of Dr. Joerg Bewersdorf at the Department of Cell Biology at the Yale School of Medicine from February to August 2016.

Dr. Warren has assisted me so much in preparing my stay and contributed greatly to my success in getting funding for my research at Yale University. He is a great supervisor, who read and graded my thesis and was a good judge of my scientific work. I am very grateful for that!

Very importantly, I want to thank Joerg of course, for providing this amazing opportunity to me, of participating in his research for half a year. He is a very kind group leader, who has trust and confidence in his lab members, even if they just stay for a short time like me. His vast knowledge about physics, biology and other matters as well as his creative way of solving problems have greatly inspired me. He was always up to date on the research I performed and gave me a ton of valuable input, when needed. Additionally, he has a lot of humor and sometimes we had a good laugh together, which made these times in his lab even more special and unforgettable.

I also want to sincerely thank Lena, my guide during my stay. She is a biologist and a mastermind. She taught me so many new techniques and passed her broad knowledge and expertise - about biology and beyond :) - on to me. Although she let me have a decent amount of freedom and autonomy of decision, all the insights I gained and the experiments I performed would not have happened without her beautiful guidance!

Next I want to thank all the members of the Bewersdorf lab with whom I share some priceless memories: Mark, Mary Grace, Michael, Emil, Andrew, Yu, Yongdeng, Xiang and Sabine. Very importantly I also want to thank Francesca Bottanelli and Myun Hwa Dunlop from the Rothman Lab who helped me so much in many regards, but especially with engineering the CRISPR cell line. Another very important person to thank is Shirin Bahmanyar. Without her help, this thesis wouldn't be what it is. She is a group leader in the Department of Molecular, Cellular and Developmental Biology at Yale University and by adding a little comment here and there she guided my experiments in the right directions. I want to thank the University of Vienna for my first step into the world of science and for offering important insights and possibilities. The second university I want to thank is of course Yale University, for supporting international scholars like me and providing them with a once-in-a-lifetime opportunity. I also want to especially thank the Austrian Marshall Plan Foundation, who kindly granted me a scholarship for my stay in the USA. Finally I also want to thank my mum and dad for supporting me my whole life long to the point where I am now. As a biologist, I admire the wonder of life from the bottom of my heart and want to express my gratitude towards Nature. I am so impressed by the molecular machines working in our bodies day after day. Especially as a microscopist, I am curious and I want to shed light on these mysteries. I am happy that I exist. And that I can wonder about such things...

Contents

List of Figures

Zusammenfassung

Das endoplasmatische Retikulum (ER) ist ein kontinuierliches Membrannetzwerk in eukaryotischen Zellen. Mit konventioneller Mikroskopie kann man drei verschiedene ER-Morphologien unterscheiden: die Kernhülle im Zentrum, umgeben von ER Zisternen und einem Netzwerk aus ER Röhrchen in der Peripherie. Elektronenmikroskopie-Studien haben allerdings detailliertere Substrukturen, wie zum Beispiel Mikro-Löcher in den ER Zisternen, offenbart. Da diese Substrukturen jedoch unterhalb der Auflösungsgrenze von konventioneller Lichtmikroskopie liegen, konnten sie noch nie in lebenden Zellen gezeigt werden.

Um diese Substrukturen in lebenden Kulturzellen zu untersuchen, habe ich eine superauflösende Lichtmikroskopie Technik verwendet: Stimulierte-Emissions-Abregungs-Mikroskopie (STED-Mikroskopie; engl. = stimulated emission depletion). Indem ich STED-Mikroskopie, gemeinsam mit Lebend-Zell-Färbe-Methoden via SNAP- und Halo-tags, anwendete, konnte ich tatsächlich mehrere Substrukturen des peripheren ERs unterscheiden.

Des Weiteren habe ich die Lokalisation von Reticulon 4 (Rtn4), einem krümmungsinduzierenden ER Protein, in lebenden und fixierten Zellen analysiert. Durch Immunfluoreszenz-Studien habe ich entdeckt, dass Rtn4 rund um Mikro-Löcher in ER Zisternen angeordnet ist, was sich sogar verstärkte, wenn die Zellen mit Nocodazole behandelt worden waren.

In Rtn4 überexprimierenden Zellen konnte ich ein eindeutiges diskontinuierliches Verteilungsmuster von Rtn4 auf den ER Röhrchen erkennen, und Artefakte wenn die Überexpression des ER Markers oder Rtn4 sehr hoch ausfiel. Um diese Überexpressions-Artefakte zu vermeiden, habe ich eine CRISPR Zelllinie, in welcher endogenes Rtn4 mit einem SNAP-tag markiert wurde, geschaffen, welche das Verteilungsmuster bestätigte.

Weil Rtn4 bekanntermaßen ER Krümmungen induziert und stabilisiert, könnte seine Assoziierung mit Mikro-Löchern bedeuten, dass es diese Substrukturen, so wie die Röhrchen und Zisternen-Ränder, stabilisiert. Das diskontinuierliche Verteilungsmuster deutet darauf hin, dass Rtn4 Krümmungen induzieren kann, auch wenn es nicht die ganze Oberfläche besetzt, was eine logische Konsequenz des Umstandes wäre, dass es auch noch andere Proteine gibt, die Platz auf der ER Membran brauchen.

Die Tatsache, dass sowohl Nocodazole Behandlung als auch die Überexpression vom ER Marker Protein zu Zisternen-Bildung führt, wohingegen die Überexpression von Rtn4 zu einem röhrchenförmigen ER führt, gibt zu erkennen, dass die ER Membran-Struktur von einem sensiblen Gleichgewicht instand gehalten wird; dies macht endogenes Markieren von Proteinen unverzichtbar.

Zusammenfassend liefern meine Ergebnisse den ersten Schritt, um die Lokalisation von Rtn4 und die Funktion der ER Substrukturen, die von Rtn4 beeinflusst werden, aufzuklären. Gleichzeitig unterstreicht meine Arbeit, wie wichtig superauflösende Mikroskopie von lebenden Zellen im Kontext dynamischer Strukturen ist.

Abstract

The endoplasmic reticulum (ER) is a continuous membrane network in eukaryotic cells. With conventional microscopy one can distinguish three different ER morphologies: the nuclear envelope in the center, surrounded by ER cisternae (sheets) and a network of ER tubules at the periphery. However, electron microscopy studies have revealed more detailed sub-structures such as micro-fenestrations in ER sheets. Because these sub-structures lie beyond the diffraction limit of conventional light microscopy, they have never been shown in living cells.

To investigate these sub-structures in living cultured cells I used stimulated emission depletion (STED) microscopy, a super-resolution light microscopy technique. By employing STED microscopy, together with live-cell labeling strategies through SNAP- and Halo-tags, I could indeed distinguish several sub-structures of the peripheral ER.

Furthermore, I analyzed the localization of Reticulon 4 (Rtn4), a reported curvature-inducing ER protein, both in fixed and living cells. By immunofluorescence studies I found Rtn4 to be arranged around micro-fenestrations in ER sheets, which was confirmed and even enhanced in nocodazole treated cells.

In cells overexpressing Rtn4 I found a discontinuous distribution pattern of Rtn4 on ER tubules, and artifacts when overexpression levels of the ER marker protein or Rtn4 were very high. To avoid overexpression artifacts, I created a CRISPR cell line of endogenous Rtn4, tagged with a SNAP-tag, which confirmed this pattern.

As Rtn4 is known to induce and stabilize ER curvatures, its association with micro-fenestrations could indicate that it stabilizes these sub-structures, just like tubules and sheet-edges. The discontinuous distribution pattern points to the fact that Rtn4 can generate curvature without fully covering the surface, which would be a logical consequence of the fact that there are also other proteins that need space on the ER membrane.

The fact that not only nocodazole treatment but also ER marker protein overexpression leads to sheet formation, whereas Rtn4 overexpression leads to a tubular ER, indicates that the ER membrane structure is maintained by a very sensitive equilibrium which makes endogenous tagging indispensable.

Altogether, my results provide a first step towards elucidating the localization of Rtn4 and the function of the ER sub-structures it influences. It also underlines how important super-resolution live-cell imaging is in the context of dynamic structures.

1 Introduction

"Structure without function is a corpse
and function without structure is a ghost."
Vogel and Wainwright (1969)

The endoplasmic reticulum (ER) is an extensive, continuous organelle that makes up about 10% of the total cell volume. It consists of a highly dynamic, interconnected membrane system, that reaches into every corner of the cell. The most important of its many functions are lipid synthesis, the regulation of the Ca^{2+} household and of course the synthesis of membrane and exported proteins (Alberts et al., 2008). As it has these and many more (probably still unknown) different functions, it is not surprising that the ER comes in a variety of different shapes.

It is divided into the nuclear envelope (NE) and the peripheral ER, which consists of cisternae (sheets) and tubules that are interconnected with each other. We can also distinguish between rough and smooth ER, where the rough ER (RER) represents ribosome-bound membranes and the smooth ER (SER) is characterized by the absence of ribosomes.

Shibata et al. (2006) propose that tubules are mostly SER and sheets usually carry ribosomes and are therefore considered RER.

Conventional light microscopy can resolve these three major compartments: tubules, sheets and the NE, which can be considered to be a flat sheet as well. Electron microscopy (EM) studies (eg. Palade (1956), Puhka (2011)), however, suggest that there is more than just sheets and tubules. Palade (Palade (1956) plate33 fig 3) described "obliquely sectioned cisternal elements" and Puhka (2011) devotes a whole section of her thesis to fenestrated ER sheets.

In this study, I examined the ER with stimulated emission depletion (STED) microscopy, a very powerful tool to investigate structures below the diffraction limit in living cells. STED microscopy, combined with suitable labeling techniques such as SNAP- and Halo-tags and membrane-permeable dyes, is live-cell compatible, which provides two unique opportunities: (1) it allows confirmation that structures observed in fixed cells also occur in living cells and (2) it allows investigation of the structure of the ER at the tens of nanometer scale and also its dynamics in real-time, without any post-processing. Only by understanding the structures, their composition and dynamics, we can start to understand and possibly discover new functions.

Here, I confirmed novel sub-structures of the ER in U2OS cells that have previously been found in the Bewersdorf lab in a different cell line and show that the

ER is a very dynamic network. Amongst the observed sub-structures, I could detect very small holes in ER sheets, hereafter called micro-fenestrations.

To investigate the role of these micro-fenestrations, I focused on ER shaping proteins. One ER shaping protein, reticulon 4 (Rtn4), belongs to the family of reticulons (Yang and Strittmatter, 2007). Together with Dp1 and maybe other factors, the reticulons are thought to stabilize curvatures in ER membranes, such as tubules and sheet edges (Voeltz et al. (2006), Shibata et al. (2006)). As a hole is a structure with high membrane curvature as well, it has been speculated that reticulons could play a role in this context (Friedman and Voeltz (2011), Hu et al. (2011)).

I looked at Rtn4 in fixed cells first and found a specific localization around micro-fenestration by immunofluorescence (IF) staining. By inducing more sheets through nocodazole treatment I could confirm this finding.

To investigate this phenomenon *in vivo* I created overexpression constructs that carried Rtn4 with SNAP- and Halo-tags to perform live-cell labeling. These live-cell experiments were unable to resolve the localization of Rtn4 around micro-fenestrations. However, I could observe interesting localization patterns of Rtn4 on the peripheral tubules: Rtn4 was not covering the tubules uniformly, but came in clusters, which indicates oligomerization as was suggested by Shibata et al. (2008).

To determine the actual endogenous localization of Rtn4, I created a CRISPR cell line carrying a SNAP tag on the Rtn4 gene. This cell line confirmed the pattern of Rtn4 distribution on tubules, though the localization of Rtn4 in sheets and their micro-fenestrations still has to be determined. The cell line will be a valuable tool to study this and, more generally, ER structure and function in the future.

In summary, I show that the ER is more diverse than previously found and that Rtn4 may localize to micro-fenestrations in ER sheets. Rtn4 definitely showed a distinct pattern on ER tubules and needs to be subject to further investigation.

2 Background

2.1 Endoplasmic reticulum and Reticulon 4

The ER is the largest organelle of a typical animal cell and contains more than half of the total amount of the cell's membrane. The ER membrane bilayer stretches throughout the whole cell and is thought to be continuous at all times (Alberts et al., 2008). The space inside this membrane is called the ER lumen and occupies more than a tenth of the whole cell volume (Alberts et al., 2008). The ER is continuous with the outer nuclear membrane. Therefore the NE envelope is considered part of the ER. The peripheral ER consists of tubules and sheets that are highly interconnected.

An additional aspect of the ER is that it can be divided into rough ER (RER), which contains ribosomes attached to the cytosolic side and smooth ER (SER), which has no ribosomes. There are also regions that are partly smooth and partly rough, which could be intermediate states between RER and SER and are therefore called transitional ER (Alberts et al., 2008). Tubules are mostly smooth and sheets are mostly rough (Shibata et al. (2006), Figure 1). The ribosomes on the RER usually cluster into large so-called polysomes, which are thought to be too big for tubules and are therefore restricted to ER sheets. Some proteins are also restricted to these sheet areas (RER proteins) whereas other proteins are thought to move freely around the ER. An additional difference between SER and RER is therefore the absence of RER proteins in SER regions (Shibata et al., 2006).

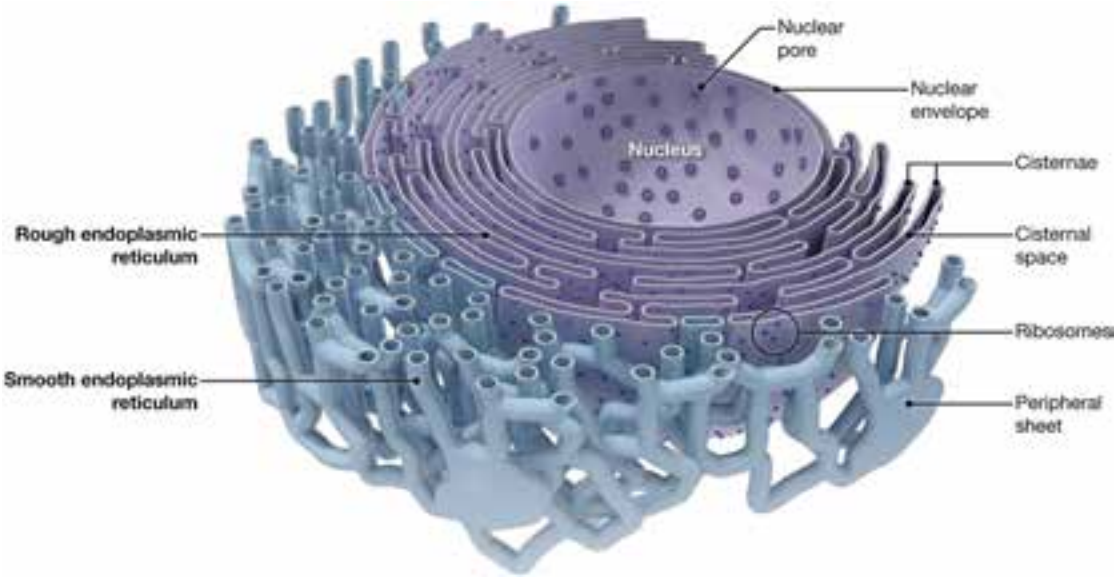

Figure 1: A schematic model of the ER, Goyal and Blackstone (2013)

The ER has many diverse functions, such as protein translocation, their folding and sorting, regulating the Ca^{2+} household, and lipid synthesis. The ER also contacts almost every other organelle (English and Voeltz, 2013). To give an example, the abscission of dividing mitochondria is triggered by ER tubules (Friedman et al., 2010).

During cell division, the NE, which is continuous with the ER, is completely disassembled and then reassembled. It is thought that the NE membranes are integrated into the ER, and after mitosis the NE is recreated from the ER (Ellenberg et al., 1997).

ER tubule growth is mediated by microtubules (MTs) by two different mechanisms: sliding and tip attachment complex (TAC) dynamics (Lee and Chen, 1988; Waterman-Storer and Salmon, 1998). In the sliding event, a growing ER tubule attaches to an existing MT and slides along the MT as it is growing. During TAC, the tip of a growing ER tubule is attached to the plus end of a MT. The ER tubule then extends together with the MT. ER tubules were already shown earlier to colocalize to a high extent with microtubules. It is surprising that despite this dependence, upon nocodazole treatment and MT disassembly, the ER tubules don't collapse immediately (Terasaki et al., 1986).

Given these diverse functions and possibly many more, it is not surprising that the ER has structurally different compartments. In order to obtain all these different structures, proteins must induce, stabilize and rearrange the conformations of the ER membrane.

Reticulons are an example for such ER shaping proteins. The family of reticulons is ubiquitously present, containing many family members from 200 up to 1200 amino acids (aa) long, in all eukaryotes (Yang and Strittmatter, 2007). Alternative splicing results in multiple isoforms of family members encoded by the same gene. Dp1 is a functionally very similar protein that shares no sequence similarity, but structural identity (Voeltz et al., 2006). They all share a carboxy-terminal reticulon homology domain (RHD) with two hydrophobic regions and a hydrophilic loop. The second hydrophobic region of the RHD is most conserved, whereas the amino-terminal domains of the reticulon proteins show little or no similarity even among paralogs within the same species (Yang and Strittmatter (2007), Figure 2).

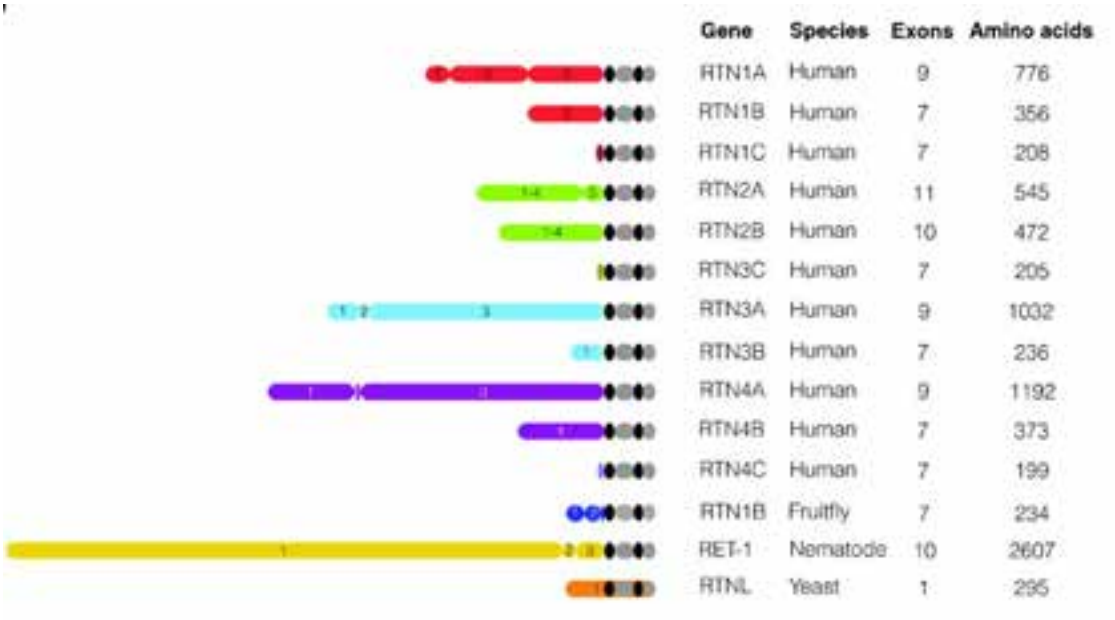

Figure 2: Schematic of the reticulon family, Yang and Strittmatter (2007), black ovals depict hydrophobic regions, colored regions are the different N-termini.

Rtn4a (or NogoA) was originally discovered as inhibitor for neurite outgrowth (hence its second name) and has been extensively studied in the central nervous system (GrandPre et al., 2000; Prinjha et al., 2000; Chen et al., 2000)).

Only later, a whole body of evidence emerged that the reticulons have a much more basic function in cellular biology, which is also supported by their ubiquitous existence. In this work, I focus on this more basic level of ER structure and the function of reticulons on a fundamental cellular level.

One hydrophobic region of the RHD is sufficient to target GFP (as a fusion protein) to the ER (Iwahashi et al., 2007). It is now thought that the RHD is the domain which exerts the basic cellular functions such as shaping membranes, whereas the diverse amino terminal domains might have more species- or cell-specific roles (Di Scala et al., 2005). The hydrophobic regions in the RHD are unusually long (30-35 aa) compared to transmembrane domains of other proteins that are usually 20 aa long (Voeltz et al., 2006). The way the reticulons insert into membranes, or if they all have the same topology, is unclear, but Voeltz et al. (2006) show that the first and maybe the second hydrophobic region of the RHD of Rtn4c adopt a hairpin structure and insert only into one of the leaflets of the bilayer, thereby bending the membrane (Figure 3A). Other possible topologies were proposed by Yang and Strittmatter (2007) (Figure 3B).

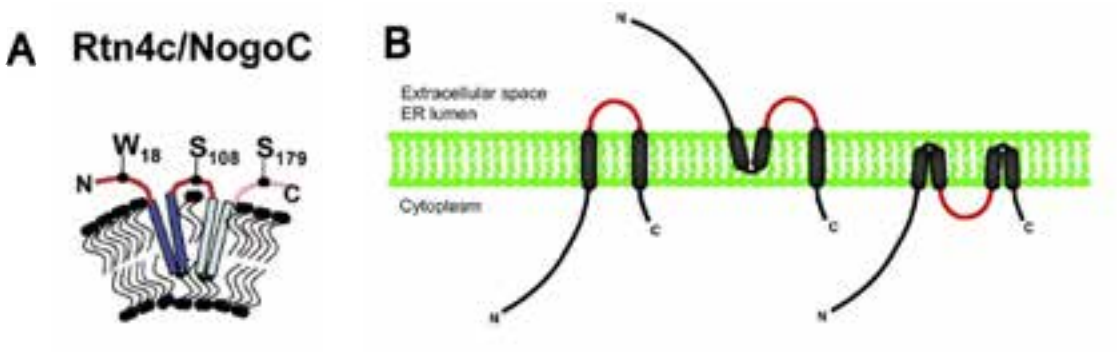

Figure 3: Schematic of the Rtn4 topology. (A) Voeltz et al. (2006) (B) Yang and Strittmatter (2007)

The Rtn4 gene encodes 3 different isoforms, Rtn4a, b and c (=Rtn4 isoform1, 2 and 3 or NogoA, B and C) (Oertle et al., 2003) (Figure 2). Human Rtn4a is only expressed in nerve tissue and is 1129 aa long. Human Rtn4b is widely expressed except for liver and is 373 aa long. Rtn4c is expressed in brain, skeletal muscle and adipocytes and 199 aa long:
`http://www.uniprot.org/uniprot/Q9NQC3`

Rtn4 is required for tubule formation *in vitro* and as all reticulons, it localizes almost exclusively to tubular ER and sheet edges, being completely absent from the NE and peripheral sheet surfaces (Voeltz et al., 2006). Overexpression of reticulons even creates more tubules and abolishes sheets (Voeltz et al., 2006). The reticulons hetero- and homo-oligomerize into arc-shaped complexes and thereby stabilize ER tubules even in the absence of MTs (Shibata et al., 2008). Only a couple of these arcs could then be sufficient to stabilize ER tubules without the need to cover the whole tubule surface. This would ensure that other proteins can still move freely (Shibata et al., 2008).

As mentioned before, the NE reforms after mitosis. Growing evidence supports a model where the NE resides in the ER during mitosis, then tubules grow to attach to chromatin and become sheets (Ellenberg and Lippincott-Schwartz, 1999). Anderson and Hetzer (2008) show that reticulons are rate-limiting for this tubule to sheet transformation, because overexpression of Rtn4 makes this process slower. siRNA knockdown makes this process faster, however, then the nucleus is smaller (Anderson and Hetzer, 2008). Reticulons also seem to be very interchangeable because three reticulons must be knocked out simultaneously for any effect on ER structures.

Reticulons are associated with a number of diseases. Nogo-A (=Rtn4a or isoform1) interacts with Nogo-R (receptor). The downstream interaction partner of Nogo-R is Rho and consequently Rock (Rho activated kinase). It has been shown that inhibition of Nogo-A-NogoR interaction leads to better recovery from spinal injury or stroke (Yang and Strittmatter, 2007), which led to clinical trials of anti-NOGO

antibody. On the other hand, the increased expression of any reticulon in the human brain reduces the production of the beta-amyloid peptide, which is the pathologic agent of Alzheimer's disease (He et al., 2004). Yet on the other hand: when Rtn1 was depleted from *C. elegans* embryos together with Yop1, it increased embryonic lethality dramatically (Audhya et al., 2007). All of these studies show that little is known about the actual function of the family of reticulons and more research needs to be performed.

In this study I decided on Rtn4b (=isoform 2) because it is expressed in all cell types except for the liver.

2.2 Stimulated emission depletion (STED) microscopy

In 1873, Ernst Abbe postulated the diffraction limit for optical instruments (Abbe, 1873) by describing the resolution as follows:

$$d = \frac{\lambda}{2n * sin\alpha} = \frac{\lambda}{2\mathrm{NA}}$$

This equation states that the distance (d =resolution) between two objects, in order to be resolved, must be greater than the wavelength of the used light (λ) divided by two times the numerical aperture (NA). The NA is an inherent characteristic of an optical system (lens), which is defined by the refractive index (n) of the sample to be imaged times the sine of the half angle of the cone of light that can enter or exit the lens ($sin\alpha$).

This means that, in theory, even if we used blue light (400 nm) and a high NA of 1.4, we could only get a resolution of about 150 nm. Due to imperfections in lenses, this theoretical limit is hard to reach. Therefore, in practice, where usually more red-shifted light of 500 nm or above is used, we can only achieve a resolution of about half the wavelength, about 200-300 nm.

Due to this diffraction limit, a point source (e.g. a single fluorescent molecule) that is recorded with an optical system, appears as a blurry spot of 200-300 nm. This is called a point spread function (PSF). In other words, the PSF is the diffraction limited image of a point source. As this diffraction limit is based on fundamental physical laws, it cannot be broken by designing better objective lenses.

Electron microscopy (EM), which was invented long ago and circumvents the diffraction limit, enabled many discoveries. However, the samples have to be fixed for EM. Therefore, an imaging technology with the spatial resolution of an electron microscope but using light, which is compatible with living samples, has long been dreamed of.

As long as only one point source emits light and we know the PSF of the optical system, we can calculate the center of the PSF and know the original position of the point source. This is the principle that is used in single-molecule localization microscopy techniques like PALM or STORM (Betzig et al. (2006), Hess et al. (2006), Rust et al. (2006)).

However, in STED, as in confocal laser scanning microscopy, we excite a multitude of fluorescent molecules at the same time. This happens because the excitation beam is subject to diffraction, just like every light beam and therefore has a minimum diameter of 200 nm, which usually excites many molecules at the same time. As multiple molecules emit light within a 200 nm spot, their images overlap and merge into one big spot. Consequently, their positions cannot be determined as in PALM or STORM.

The principle of stimulated emission depletion (STED) microscopy was proposed by Stefan Hell as early as in 1994 (Hell and Wichmann, 1994), an invention for which he won the Nobel Prize in Chemistry in 2014. The key idea behind STED microscopy is to confine the space from which molecules emit light to a space much smaller than the diffraction limit. Even though their images will be blurred in detection, their location in the sample is then known as long as the position of the confined space is known. This space confinement is achieved by switching off molecules that reside outside of the very center of the excitation beam immediately after they have been excited and before they can emit any fluorescence.

In conventional confocal microscopy, usually molecules are imaged which emit fluorescence (Figure 4A). A fluorescent protein or dye molecule can be excited with short wavelength light (=high energy photons) and thereby transferred from the ground state to an excited electronic state. Within picoseconds it undergoes vibrational relaxation to a lower vibrational energy level but still remains in the excited electronic state. From there it relaxes back to the ground state emitting a photon of a longer wavelength with lower energy. This is called spontaneous emission and occurs on the order of nanoseconds. The emitted photon can be anywhere in the range of the emission spectrum (Figure 5).

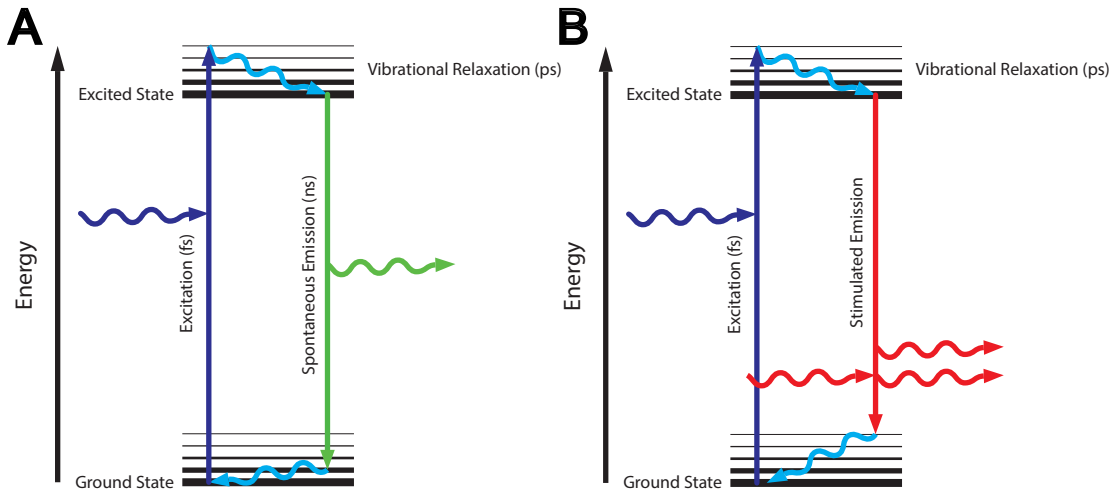

Figure 4: Energy diagram of spontaneous and stimulated emission. (A) A fluorescent molecule gets excited by a photon of a certain wavelength and relaxes back down to the ground state whereby it emits a photon of a higher wavelength (=lower energy). (B) A fluorescent molecule gets excited by a photon of a certain wavelength and before it relaxes back down to the ground state a second photon of much lower wavelength is introduced. This forces the molecule back to the ground state whereby it emits two photons of the same wavelength as the one that was introduced. Image courtesy of Edward Allgeyer.

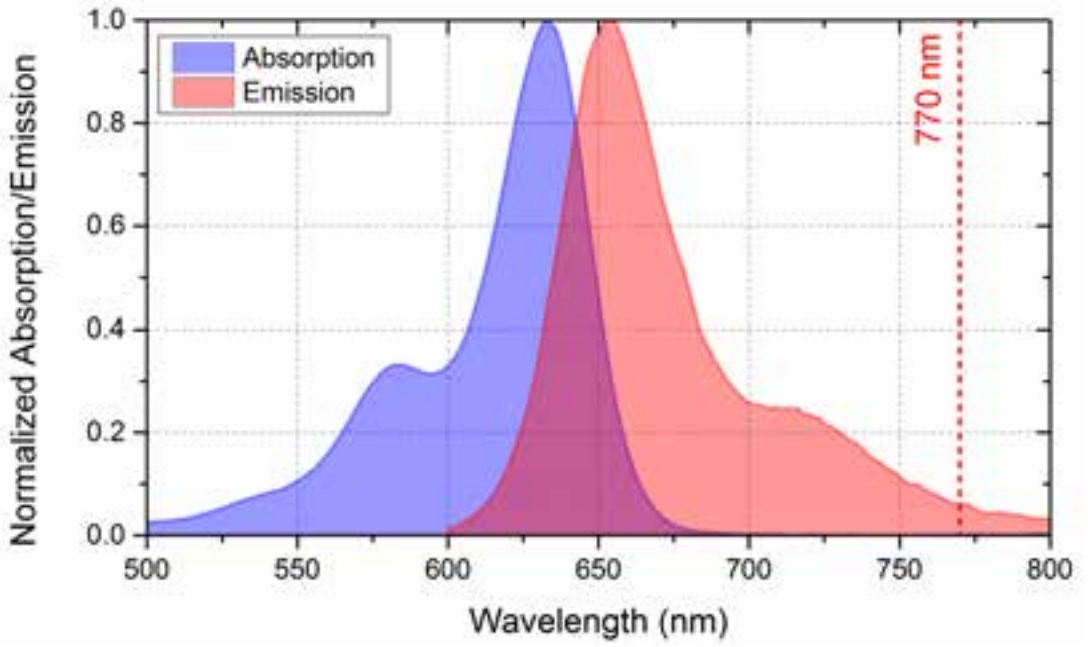

Figure 5: Excitation/emission spectrum of a fluorescent dye with depletion line (770nm). Image courtesy of Edward Allgeyer.

In order to suppress the emission of fluorescence, the concept of stimulated emission is applied in STED microscopy (Figure 4B). A photon of light with usually longer wavelength (=lower energy) than most fluorescence photons interacts with the fluorophore while it still resides in the excited state. The lower energy of this

STED photon fits the energy gap between the excited and ground state of the fluorophore and is just enough to force it to the ground state. The interaction has to take place during the couple of nanoseconds the fluorophore resides in the excited state. While the fluorophore is then coming back to the ground state, it is emitting a second photon of the exact same wavelength as the photon that stimulated that emission. Both of these photons with this longer wavelength are not recorded by our detectors and the fluorophore therefore appears switched off.

To achieve this STED effect, an additional laser is used, which emits light of a wavelength that corresponds to the red tail of the spectrum of the used fluorophore (Figure 5).

This depletion laser or STED laser, passes through a phase mask, that creates a donut shaped STED focus centered on the excitation laser focus. In the middle of the donut, the intensity of the STED beam is very small (ideally zero) and therefore molecules at that location can stay in the excited state and emit fluorescence, while all the others around them are depleted (Figure 6).

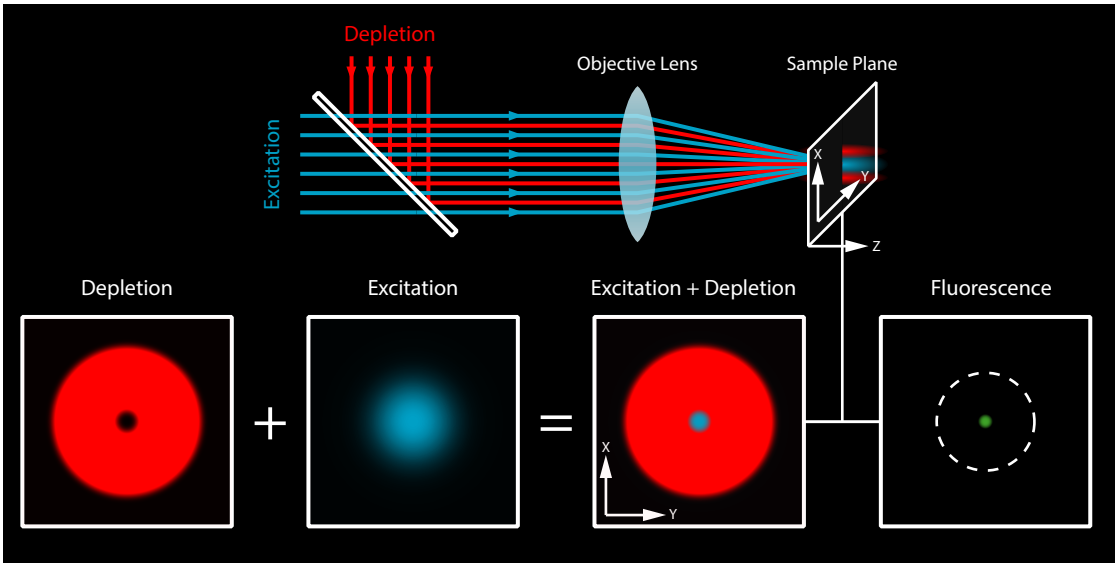

Figure 6: Simplified cartoon of a STED microscopy setup. An excitation laser (blue) brings the fluorophores to an excited electron state just like in conventional confocal fluorescence microscopy. The fluorophores would then usually relax back to the ground state by emitting light of a longer wavelength (green), a process called fluorescence. In a STED microscope, however, an additional laser with a wavelength at the red tail of the fluorophore emission is introduced into the microscope. This depletion laser (red) passes through a phase mask that produces a donut shaped focus centered on the excitation laser focus. The red donut pattern is shown saturated since the STED power is chosen high enough that even relatively low STED laser intensities are sufficient to switch off most molecules. Thereby the area which can actually emit light is limited to a very small portion of the initial excitation spot and resolution is therefore greatly enhanced. The image is scanned in a raster format. So for every position that is scanned the collected photons are attributed to the spot where they came from, i.e. the center of the depletion donut. Image courtesy of Edward Allgeyer.

The co-aligned excitation and depletion lasers are scanning across the sample with a scan speed of, for example, 8000 Hz. Therefore at every position recorded, a separate subset of molecules emits fluorescence. The fluorescence is recorded by the detector as photon counts sequentially in time. Usually avalanche photo diodes or HyD detectors (Anzivino et al. (1995), `http://www.leica-microsystems.com/products/confocal-microscopes/technology/hyd/`) are used instead of the conventional photo multiplier tubes common for confocal microscopy. Because of the raster scanning format, the recorded fluorescence can be attributed to a distinct spot on the scan field and a corresponding image is built up point-by-point.

To make sure that the vast majority of molecules will be depleted outside of the center spot, a lot of STED photons are needed. This is controlled by the intensity of the STED beam, which influences the achievable resolution and Abbe's equation has to be modified accordingly (Hell and Wichmann (1994)):

$$d = \frac{\lambda}{2n * sin\alpha * \sqrt{1 + \mathrm{I}/\mathrm{I}_s}}$$

The more the STED laser intensity (I, of the order of MW/cm^2) exceeds the characteristic saturation intensity (I_s) of the imaged fluorescent probe, the smaller the PSF and the better the resolution (therefore the distance (d) between two objects that can be resolved) gets. The STED effect can be demonstrated by imaging small crimson beads, which appear as having a 300 nm diameter in confocal (Figure 7A)and around 75 nm in STED with the setup I was working with (also limited by the size of the used beads; Figure 7B). In other setups, the resolution can be as low as 25 nm. Some beads appear very big and bright in the confocal mode, and only in STED we can see that they are actually two or more beads blurred together (Figure 7B, lower panel).

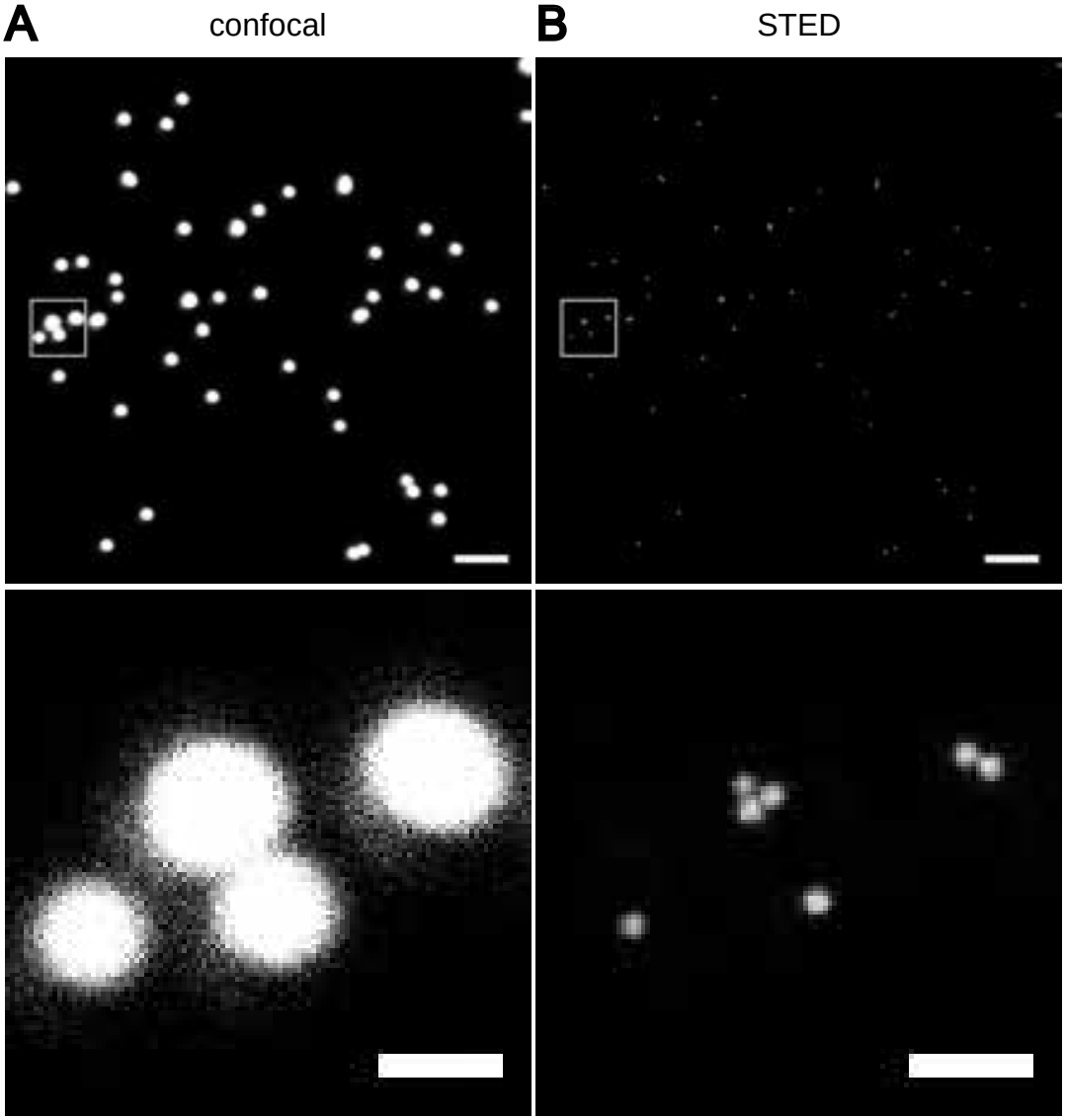

Figure 7: Resolution comparison between confocal and STED: 100 nm Crimson beads were recorded in (A) confocal and (B) STED mode. Scale bars: 2 and 0.5 µm.

In conclusion, the scanning of a sample with co-aligned excitation and STED lasers leads to a spatially separated, sequential recording, just like in conventional scanning confocal microscopy, but with increased resolution due to the space confinement of the emitted fluorescence to a smaller spot size. Although diffraction itself cannot be eliminated, the barrier that was set by diffraction has been overcome by STED. Instead of trying to create narrower beams with better lenses STED microscopy uses two different states of fluorescent molecules.

A good explanation of this is given by Stefan Hell in this iBiology-video:
`https://www.ibiology.org/ibioeducation/taking-courses/super-resolution-overview-and-stimulated-emission-depletion-sted-microscopy.html`

2.3 SNAP- and Halo-tag technologies and STED dyes

Two general strategies to label cells are widely used:
1) The cell can either be fixed and then labeled with indirect immunofluorescence (IF), where the secondary antibody (AB) carries a dye molecule.
2) Or the cell can overexpress a fusion-protein which has a fluorescent protein as tag.
Although the first strategy is suitable and widely used for STED microscopy, it usually only works with fixed samples. The fluorescent proteins of the second strategy are mostly not suitable for STED because they cannot be depleted easily, or they are not photo-stable. In order to perform live-cell STED imaging, a different labeling strategy is advantageous. I utilized the SNAP- and Halo-tag technology following Bottanelli et al. (2016). The SNAP-tag® (Figure 8A, NEB, Keppler et al. (2003)) and the HaloTag® (Figure 8B, Promega, Los et al. (2008)) technologies are both novel tools based on protein tags that can be specifically labeled with synthetic fluorophores. This has two major advantages over conventional fluorescent protein tags: Firstly, synthetic dyes come in a broader range of colors and are more photo-stable and usually brighter than fluorescent proteins. Secondly, one single fusion protein can be flexibly labeled with different colors without having to engineer many different fusion products of the same protein.

In a two-step process, the cells are first engineered to (endogenously or over-) express a fusion protein composed of the protein of interest and a Halo- or SNAP-tag. The cells are then labeled with STED-compatible dyes (see section 5.6.3) that form a covalent bond with those tags (see Figure 8). The two dyes, silicone rhodamine (SiR, Figure 8C, Lukinavicius et al. (2013)) and Atto590 (A590, Figure 8D) were mainly used. To covalently bond with the tags they need a specific substrate: benzylguanine (BG) is the substrate for SNAP-tag and chloroalkane (CA) for Halo-tag. SiR-BG was obtained from NEB (SNAP-Cell® 647-SiR S9102S), SiR-CA was kindly distributed by Promega. A590-BG was made by Roman Erdmann (Schepartz lab) and A590-CA was made by Alex Thompson (also Schepartz lab).

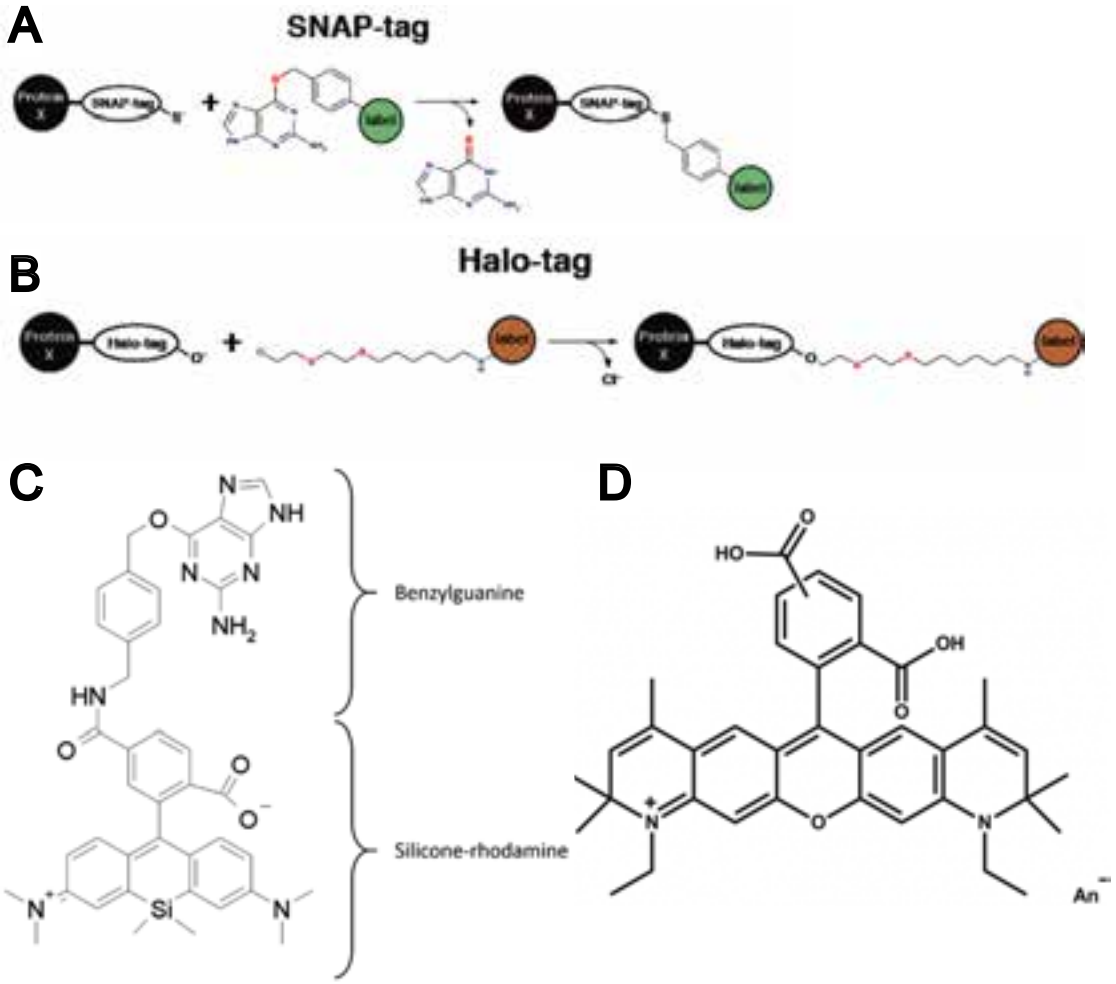

Figure 8: Tags and dyes (A) SNAP tag: A fluorophore (=label) is coupled to the small substrate benzylguanine in order to be bound by the SNAP-tag which is expressed as a fusion protein with a protein of interest (Protein X). Upon bond formation guanine is released. (B) Halo-tag: A fluorophore (=label) is coupled to the small substrate chloroalkane in order to be bound by the Halo-tag which is expressed as a fusion protein with a protein of interest (Protein X). Upon bond formation a chloride ion is released. (C) Chemical structure of SNAP-Cell® 647-SiR (=SiR-BG): Silicone-rhodamine (lower bracket) is coupled to benzylguanine (upper bracket). (D) Chemical structure of Atto590 without any substrate. (A) and (B): Adapted from Kohl et al. (2014).

2.4 CRISPR

Modifying the genome and introducing certain mutations, such as single base pair deletions, insertions or even the introduction of whole new genes is relatively easy with the new technique of CRISPR (Ran et al., 2013). I used this technique to introduce a tag into the genome of my cell line, which was C-terminally coupled to my gene of interest to produce a fusion protein which can be labeled with the dyes through the SNAP-tag technology as mentioned in section 2.3.

3 Results

For my work, I selected U2OS cells, an osteosarcoma cell line, for the most part of my experiments, because they are very flat and therefore very suitable for super-resolution microscopy. Additionally it was attractive to work in a cell line with human background. This was also a major advantage for the CRISPR tagging, because most CRISPR editing has been performed in the human genome so far.

3.1 STED microscopy reveals ER sub-structures beyond the diffraction limit

A typical ER tubule measures less than 100 nm in diameter. This size lies well below the diffraction limit of conventional microscopy. However, most ER morphologies to date have been described based on confocal microscopy, or they have been investigated with EM, using fixed samples. To determine distinct ER sub-structures in living cells, the commonly used ER marker Sec61β (the β subunit of the Sec61 translocator) with a Halo-tag was overexpressed in U2OS cells. The tag was labeled with the dye SiR-CA before imaging. STED microscopy revealed structural features otherwise not observable. Consistent with Schroeder et al. 2016 (unpublished data), I was able to discriminate between four different sub-types of ER shapes that have never been resolved in living cells before (Figure 9). These sub-structures included bundled tubules, loop junctions, clustered junctions and micro-fenestrations in ER sheets (Figure 9 B). Bundled tubules are two or more parallel ER tubules, which appear as either thick tubules or even sheets when recorded in confocal mode. Loop junctions are junctions between tubules that appear as small sheets in confocal microscopy, but are actually tubules that form a loop or ring as a junction between usually three or more tubules. Clustered junctions and fenestrated sheets both appear as uniform sheets in a confocal image. However, clustered junctions consist of many short interconnected tubules, whereas fenestrated sheets are ER sheets containing micro-fenestrations, where the distance between the micro-fenestrations is bigger than a typical tubule diameter (Schroeder et al. 2016 unpublished data). Many intermediate stages between these four sub-structures could also be found in each cell. This result demonstrates that high resolution without post-processing can be achieved with STED, which reveals ER sub-structures beyond the conventional confocal resolution.

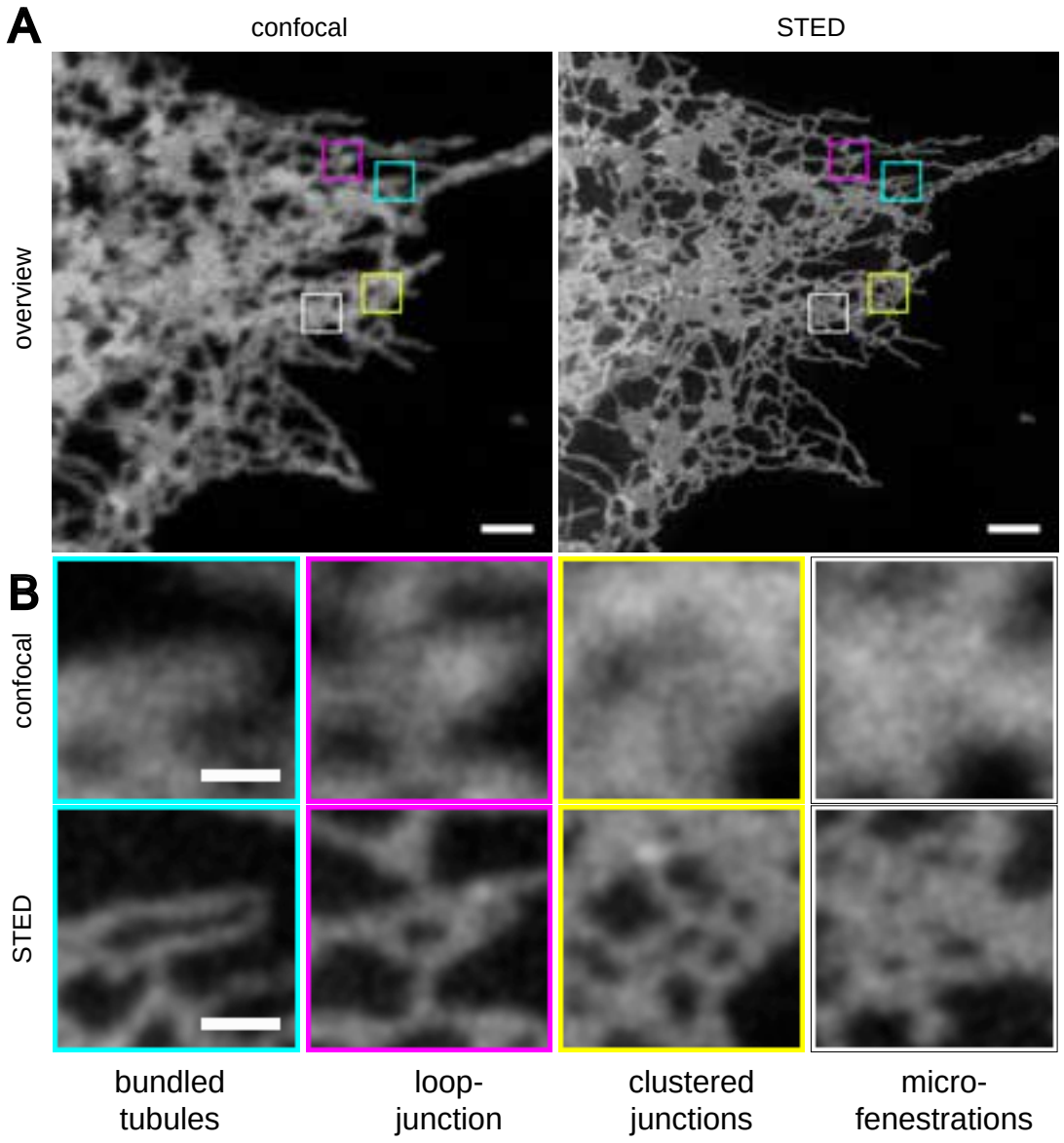

Figure 9: Sub-structures of the ER can be resolved by STED. (A) shows an overview of a cell that was overexpressing Halo-Sec61β and was live-labeled with SiR-CA after 24 hours of expression. (B) shows magnified areas of distinct sub-structures boxed in (A). The upper panel shows the confocal images and the lower panel shows the corresponding STED images. Scale bars: (A) 2 µm, (B) 0.5 µm.

3.2 STED imaging resolves nanoscale temporal dynamics of the ER

It is not only crucial to image the ER with high resolution but also to capture the fast movements of this highly dynamic organelle. For this reason, movies of living cells were taken over the course of 60 sec (Figure 10). I looked at the ER marker Sec61β with a Halo-tag which was overexpressed in U2OS cells and labeled with SiR-CA. STED images of the same position in the same cell were taken at time points that were about eight seconds apart. I could observe highly dynamic rearrangements of the ER from one time point to the next. A good indication of cell viability was the continuous movement that persisted until the end of the movie. A tubule can be observed as it is emerging after 30 seconds and continuously extending until the end of the movie (Figure 10B). Loop junction dynamics are magnified in Figure 10C and micro-fenestration rearrangements in sheets can be found in Figure 10E. All of these dynamic rearrangements would not be distinguishable at confocal resolution. Altogether, these observations indicate that STED microscopy is an adequate tool to observe ER sub-structures beyond the diffraction limit and their highly dynamic movements.

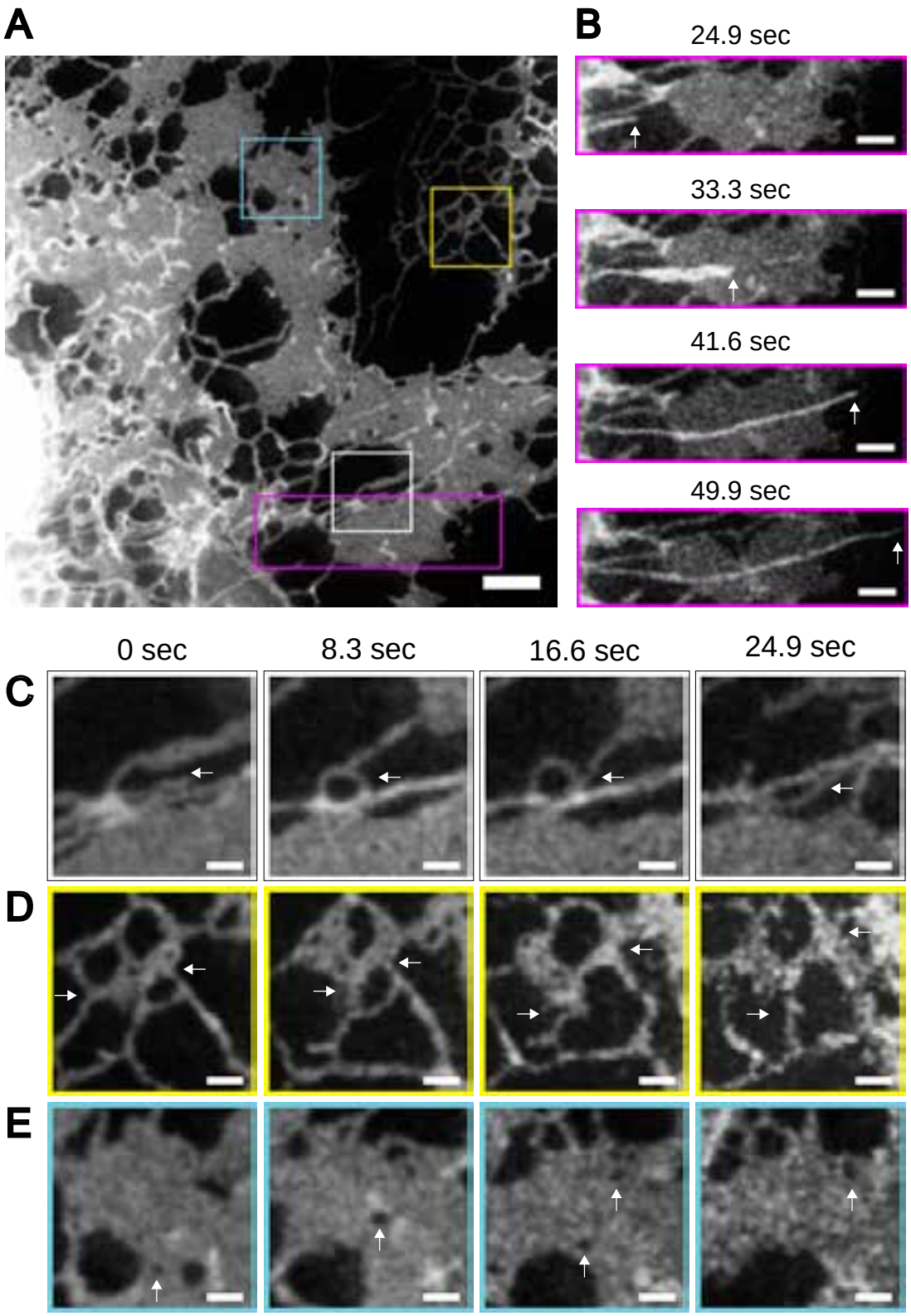

Figure 10: live-cell STED imaging of dynamic structures of the ER. (A) Overview of cells that were overexpressing Halo-Sec61β and live-labeled with SiR-CA after 24 hours of expression. Small areas boxed in (A) are magnified in (B-E). (B) Tubule emerging. (C) Loop junction formation. (D) Clustered junction rearrangements. (E) micro-fenestration dynamics in ER sheet. (B-E) Arrows point to sites of interest. Scale bars: (A) 2 µm, (B-E) 0.5 µm.

3.3 Similar ER sub-structures can be observed in multiple cell types

Next, I tested whether the described sub-structures occurred universally. For this purpose, I imaged different cell types to investigate if their ER also contained similar sub-structures. All three cell types that were examined, U2OS, COS7 and HeLa cells, showed comparable features. However, consistent with Puhka (2011) the micro-fenestrations seem to have different sizes, shapes and abundances (Figure 11). This finding shows that sub-structures such as micro-fenestrations in ER sheets might be a universal but varying phenomenon in different cell types.

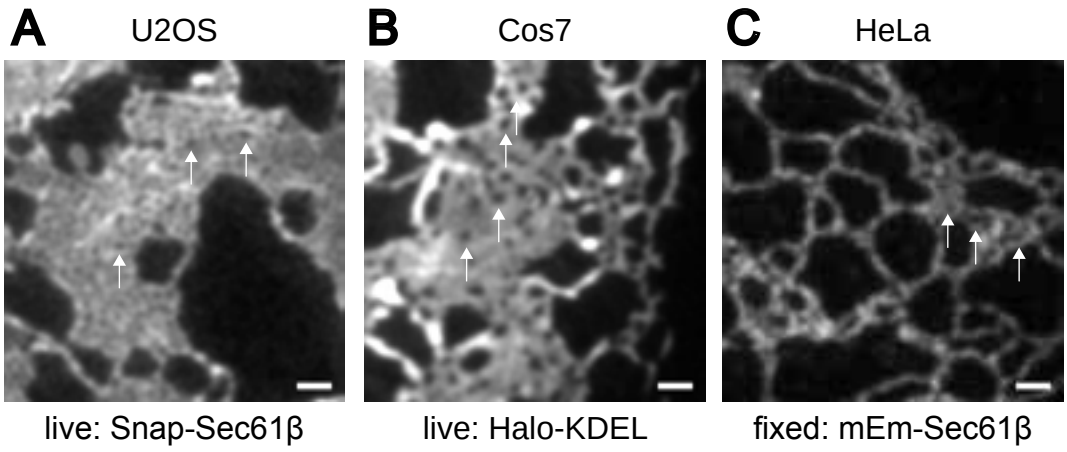

Figure 11: Images of the ER in different cell types show micro-fenestrations to be a universal phenomenon. (A) Live U2OS cell: The overexpressed ER marker SNAP-Sec61β was live labeled with SiR-BG. (B) Live Cos7 cell: The overexpressed ER marker Halo-KDEL was live labeled with SiR-CA, image courtesy of Lena Schroeder. (C) Fixed HeLa cell: The ER-marker Sec61β was overexpressed with a mEmerald tag and indirect IF was performed with a primary anti-GFP antibody and a secondary antibody coupled to the STED dye Atto647N. Scale bars: (A-C) 0.5 µm.

3.4 Rtn4 localizes around micro-fenestrations in fixed cells

To further investigate the function of these micro-fenestrations, I examined Rtn4, a curvature-stabilizing protein. To this end I fixed SNAP-Sec61β overexpressing cells and determined the localization of Rtn4 by indirect immunofluorescence (Figure 12). Consistent with previous findings (Voeltz et al. (2006)), Rtn4 localized to tubules and seemed to be more prominent at the periphery than the overexpressed Sec61β. The Rtn4 staining on the tubules appeared discontinuous, which could be real or due to the fact that an antibody staining is not 100% efficient. Rtn4 also localized to the edges of ER sheets, but seemed to be mostly excluded from the central sheet area (Figure 12 A). When taking a closer look however, in sheets that contained micro-fenestrations, Rtn4 also appeared to localize specifically to the edges of micro-fenestrations (Figure 12 C). To validate this, I plotted the gray values of the two different channels (Sec61β and Rtn4) against their position along a straight line through the ER (Figure 12D). The two micro-fenestrations can be identified as the minima in the magenta dataset, which represents Sec61β. The green dataset shows Rtn4 whose maxima are the same distance apart as the half minimum of the Sec61β dataset. This indicates that Rtn4 was most abundant at a position where Sec61β was at half its intensity, which represents the edge of a micro-fenestration. Both datasets have overlapping minima. The plot therefore suggests that Rtn4 could indeed line the micro-fenestrations but not fully occlude them. The Rtn4 dataset shows that the second micro-fenestration has an imperfect lining with Rtn4. This could be due to the aforementioned impairments of an antibody staining or because not every micro-fenestration has a continuous lining with Rtn4. Some areas in the sheets were completely devoid of Rtn4 staining. These areas frequently coincided with areas of the sheets without micro-fenestrations. Rtn4 might therefore be an important factor in micro-fenestration function and could be a good tool to distinguish fenestrated sheet areas from uniform sheet areas. All of these observations could only be made through the application of STED microscopy, because confocal images of the same region are too blurred to distinguish any shapes (Figure 12 B).

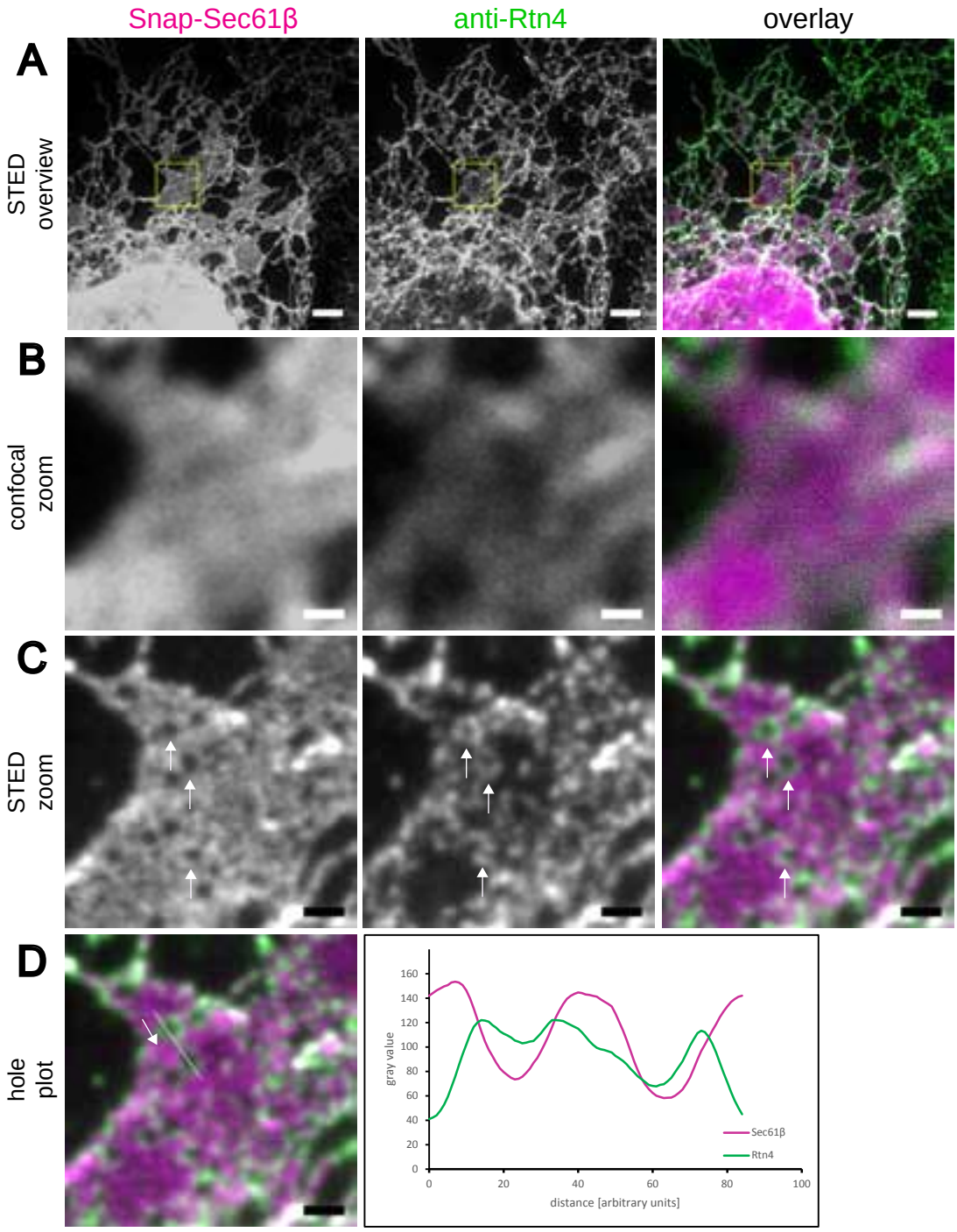

Figure 12: Fixed cell STED images of Sec61β and Rtn4. (A) The overexpressed ER marker SNAP-Sec61β was live labeled with SiR-BG (magenta) and Rtn4 was visualized by indirect IF with a specific primary antibody and a secondary antibody coupled to the STED dye Atto594 (green). (B) Confocal magnifications of the boxed region in (A). (C) The same region in STED. Arrows point at micro-fenestrations containing Rtn4. (D) A plot over two holes to demonstrate that Rtn4 lines the micro-fenestrations. Scale bars: (A) 2 µm, (B-D) 0.4 µm.

To test whether the overexpression of Sec61β had any effect on the localization of Rtn4, I fixed non-transfected wildtype cells and co-immunostained them for Rtn4 and the endogenous ER marker KDEL. While these cells tended to show less ER sheets than the cells overexpressing Sec61β, Rtn4 showed a similar pattern of localizing to ER tubules and micro-fenestrations in ER sheets. (Figure 13).

Combined, these observations are a first step toward elucidating the function of micro-fenestration and one of the involved proteins, Rtn4.

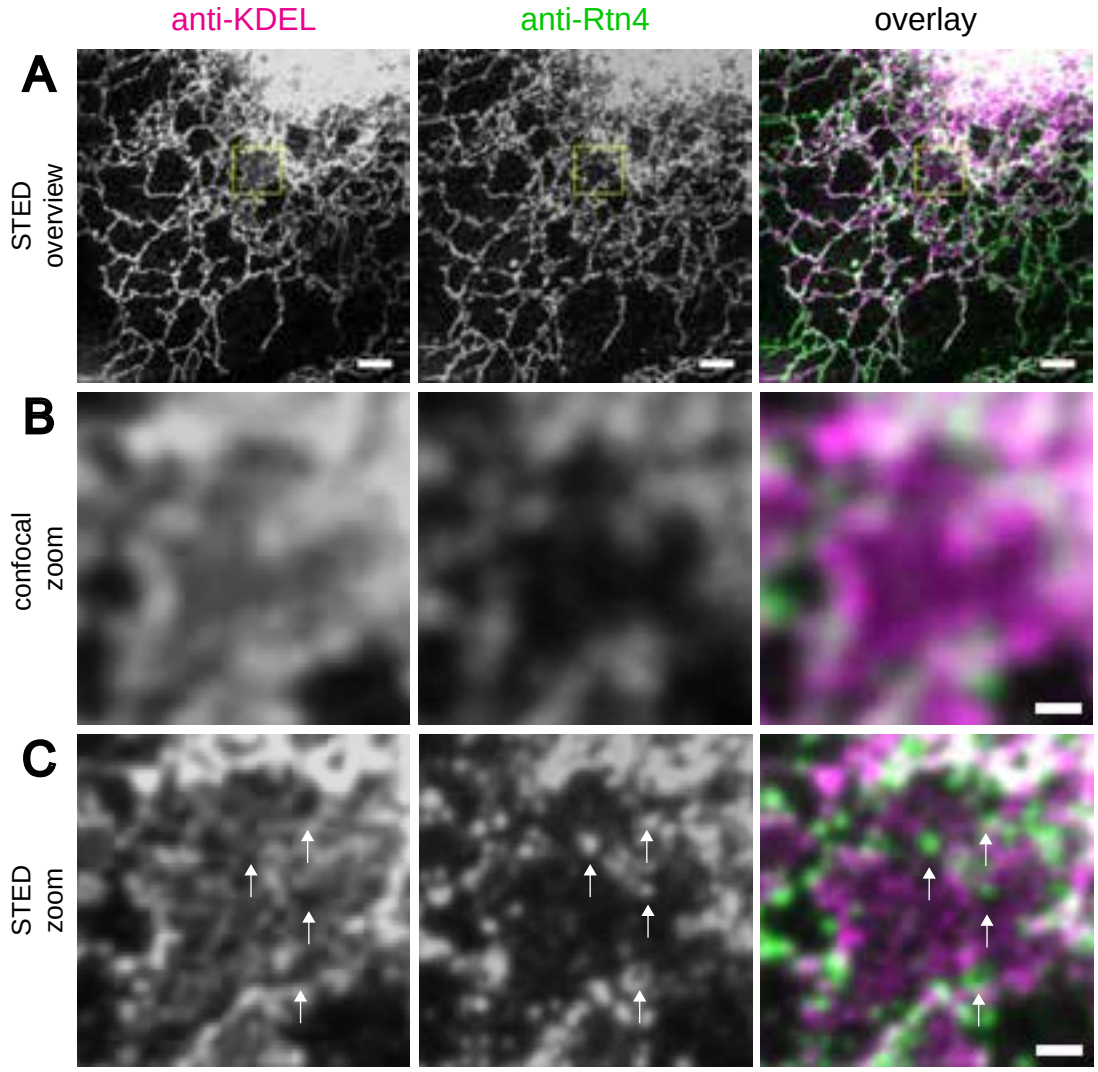

Figure 13: Fixed cell STED images of KDEL and Rtn4. (A) The ER marker KDEL and Rtn4 were visualized by indirect IF with specific primary antibodies. The secondary antibody for KDEL was coupled to the STED dye Atto647N (magenta) and for Rtn4 we used Atto594 (green). (B) Confocal magnifications of the boxed region in (A). (C) The same region in STED. Arrows point at micro-fenestrations containing Rtn4. Scale bars: (A) 2 µm, (B-C) 0.4 µm.

3.5 Nocodazole treatment supports the localization of Rtn4 around micro-fenestrations in fixed cells

To gain deeper insight into the function of Rtn4, I perturbed the system by increasing the ER sheet area. This was achieved by nocodazole treatment, which leads to disassembly of the microtubules and thereby to a decrease in ER tubules and an increase in sheets (Terasaki et al. (1986)). In the resulting cell whose ER mainly consists of sheets, the localization of Rtn4 was determined. For this purpose, Sec61β overexpressing cells were labeled with SiR-BG and then treated with 33 µM nocodazole. After 30 min of treatment the cells were fixed and stained for Rtn4 with a specific antibody (Figure 14). The left image in Figure 14 A shows the typical cell morphology I observed after nocodazole treatment. The cells had extended sheet areas and almost no tubular structures left. The right images show a confocal and STED overview of a region of the same cell where Rtn4 seemed to be dispersed or run like a network throughout the whole ER sheet. At a closer look however, these ER sheets of nocodazole treated cells appeared very fenestrated, with many of these micro-fenestrations specifically surrounded by Rtn4 (Figure 14 C, corresponding confocal in B). Again, some areas that seemed to contain less or no micro-fenestrations, showed no Rtn4 staining; they were substantially less abundant than in untreated cells though (compare to Figure 12). These findings indicate that nocodazole treatment induces highly micro-fenestrated ER sheet formation and most of these micro-fenestrations appear to be outlined by Rtn4.

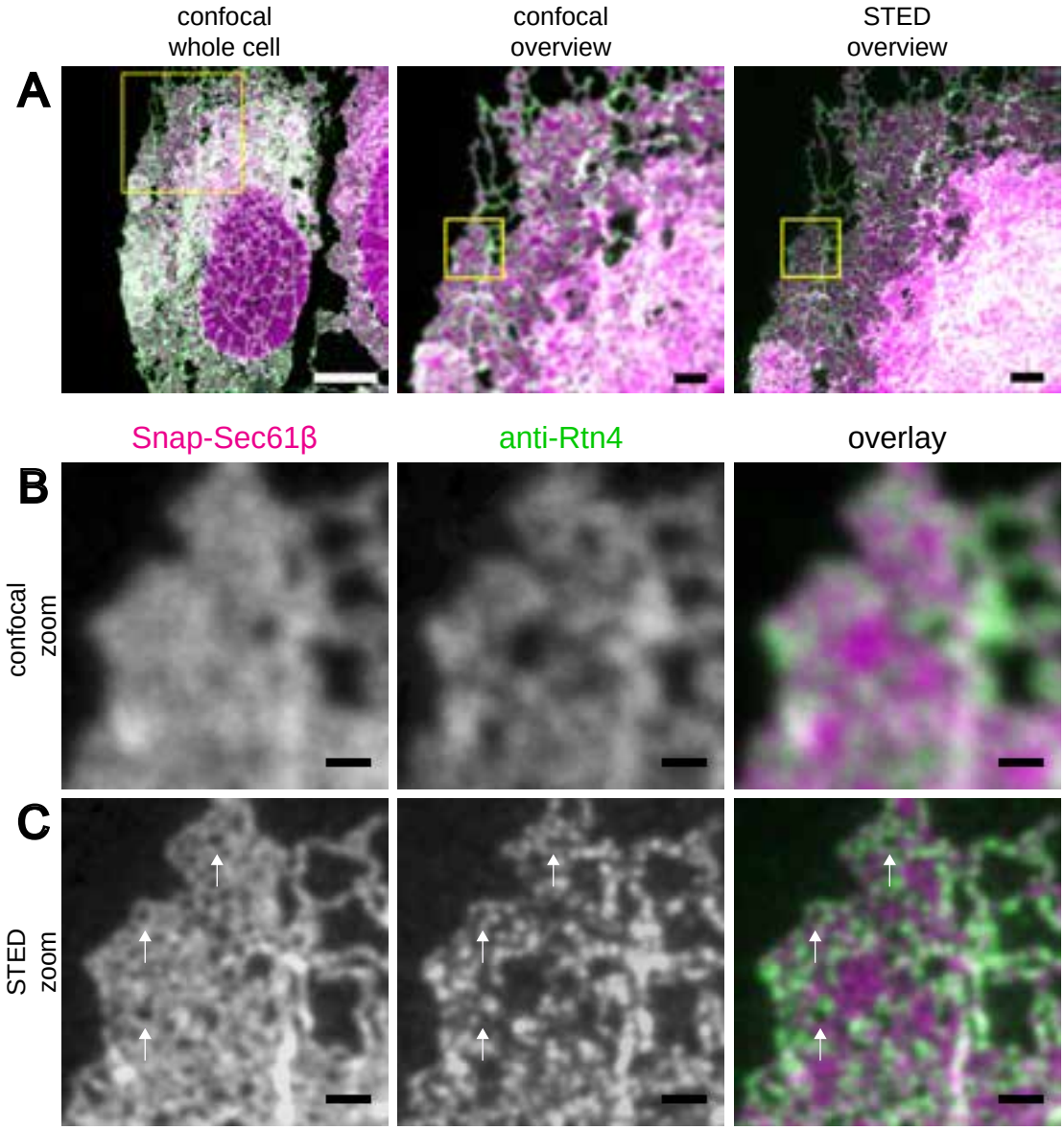

Figure 14: Fixed cell STED images of the ER and Rtn4 in nocodazole treated cells. The overexpressed ER marker SNAP-Sec61β was live labeled with SiR-BG. The cell was treated with 33 µM nocodazole for 30 min. Rtn4 was visualized with a specific primary antibody and a secondary antibody coupled to the STED dye Atto594. (A) Whole cell image and region overviews in confocal and STED mode. (B) Confocal magnifications of the boxed region in the left panels in (A). (C) The same region in STED. Arrows point at micro-fenestrations containing Rtn4. Scale bars: (A) 10 µm and 2 µm, (B-C) 0.5 µm

3.6 Tug of war beween Rtn4 and Sec61β overexpression

To review these findings *in vivo* and to rule out the artifact of fixation, I tested the localization of Rtn4 in live-cells. For this purpose, I made four different expression plasmids of Rtn4, either carrying a C- or N-terminal SNAP- or Halo tag (Supplementary figure S1A). The cells were then live labeled with A590-BG or A590-CA, respectively, and imaged. The Halo-tagged Rtn4 plasmids seemed to result in the expected morphology in contrast to the SNAP-tagged ones (see Supplementary figure S1B). I could not determine any difference between N and C terminally tagged Halo plasmids and they were therefore chosen for future experiments. In accordance with Voeltz et al. (2006), Rtn4 overexpression seemed to cause the ER in most cells to become mostly tubular (Figure 15).

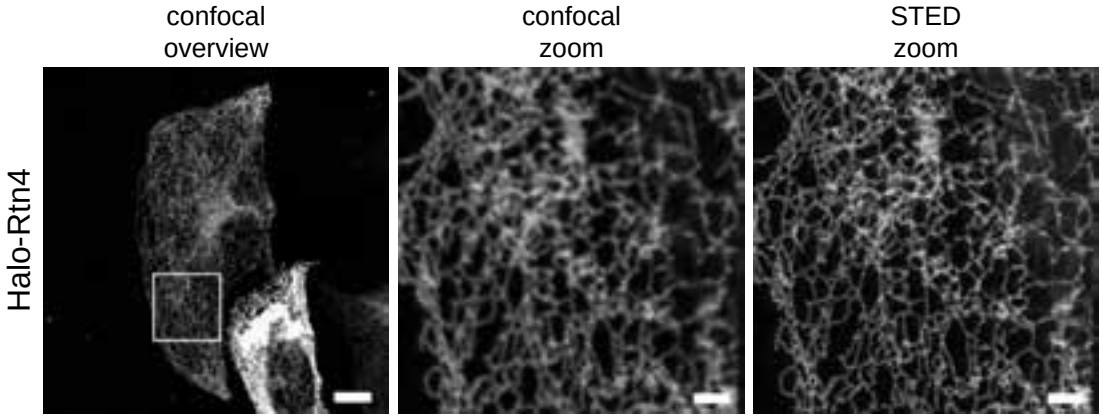

Figure 15: Live STED image of Rtn4. Overexpressed Halo-Rtn4 was live-labeled with A590-CA. Left panel shows a confocal overview of the whole cell and right panels show the boxed region in confocal and STED resolution. As in all following live-cell images, one could detect a slight difference between the overview and the zoom images because the living cell had moved from one shot to the next. Scale bars: 10 and 2 µm.

When the cells coexpressed Sec61β at a moderate level (Figure 16A and B), some ER sheets could be found that were contoured by Rtn4. However, they were very sparse and too small to find any micro-fenestrations in them. Interestingly, as in the fixed cell images, I could observe a discontinuous pattern of Sec61β and Rtn4 on tubules (Figure 16C). Voeltz et al. (2006) state that Rtn4 displaces Sec61β from the peripheral ER. To test whether these two proteins were distributed in an anti-correlative manner, I plotted the protein distribution of three different tubules and calculated their Pearson coefficient (Figure 16D). Two out of three tubules showed a tendency for an anti-correlated distribution and one appeared to be randomly distributed. This leaves room to speculate about mutual exclusion of of Sec61β and Rtn4, as was suggested by Voeltz et al. (2006).

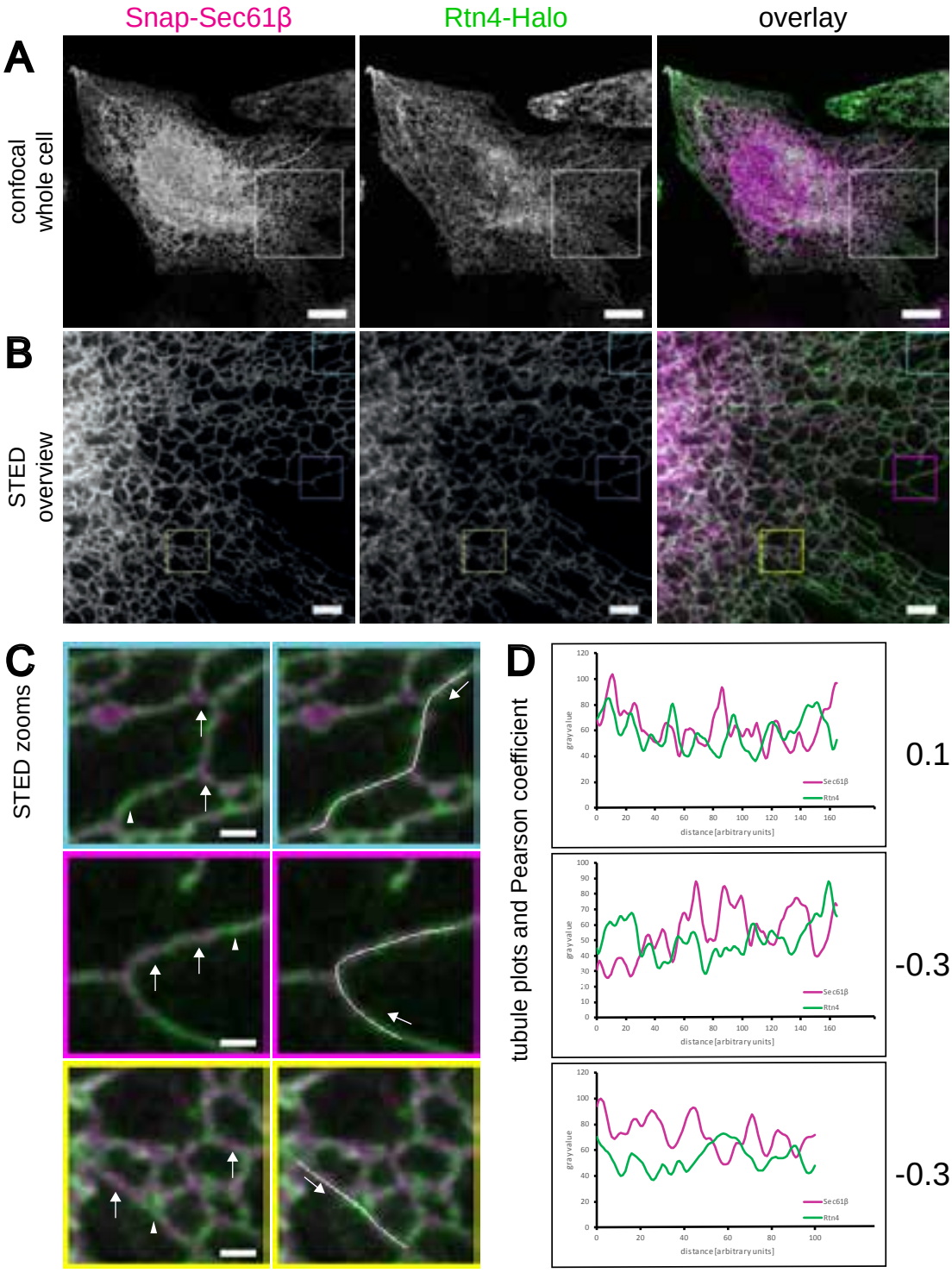

Figure 16: Live STED image of Sec61β and Rtn4. SNAP-Sec61β and Rtn4-Halo were labeled with SiR-BG and A590-CA, respectively. (A) Confocal overview of the whole cell. (B) Overview of the boxed region in (A). (C) Boxed regions from (B). Left panels: arrows point to positions which show primarily Sec61β staining. Arrow heads point to predominantly Rtn4 containing positions. Right panels depict the line that was drawn through the individual tubules; arrow marks beginning of plot. (D) The corresponding plots to the lines in (C). Sec61β in magenta and Rtn4 in green. The Pearson coefficient of each plot is calculated and shown next to the graphs. Scale bar: (A) 10 µm, (B) 2 µm, (C) 0.5 µm.

To investigate the interaction of Sec61β and Rtn4, I compared cells with different expression levels of the two proteins (Figure 17A). When Rtn4 levels were higher than Sec61β (Figure 17B) the ER consisted almost exclusively of tubules that were densely clustered and hardly any sheets could be observed. The discontinuous distribution pattern of Sec61β and Rtn4 could be observed again (Figure 17C).

Notably, when cells were highly overexpressing Sec61β and had comparably lower levels of Rtn4 (Figure 17D), the tubule-inducing properties of Rtn4 could be partially reversed, leading to increased sheet formation. However, while Rtn4 localized beautifully to the tubules, it randomly localized throughout the whole sheet areas, with some exceptions. Rtn4 even showed unspecific localization in bigger holes in the ER. It is therefore unclear whether it had some specificity to the microfenestrations (Figure 17E), as it was observed by IF.

Together these results suggest that depending on higher expression levels of either Rtn4 or Sec61β, the cells have more tubules or sheets, respectively. However, even upon sufficient Sec61β overexpression to form sheets, an absolute answer to the localization of overexpressed Rtn4 in live-cells in the context of microfenestrations could not be found.

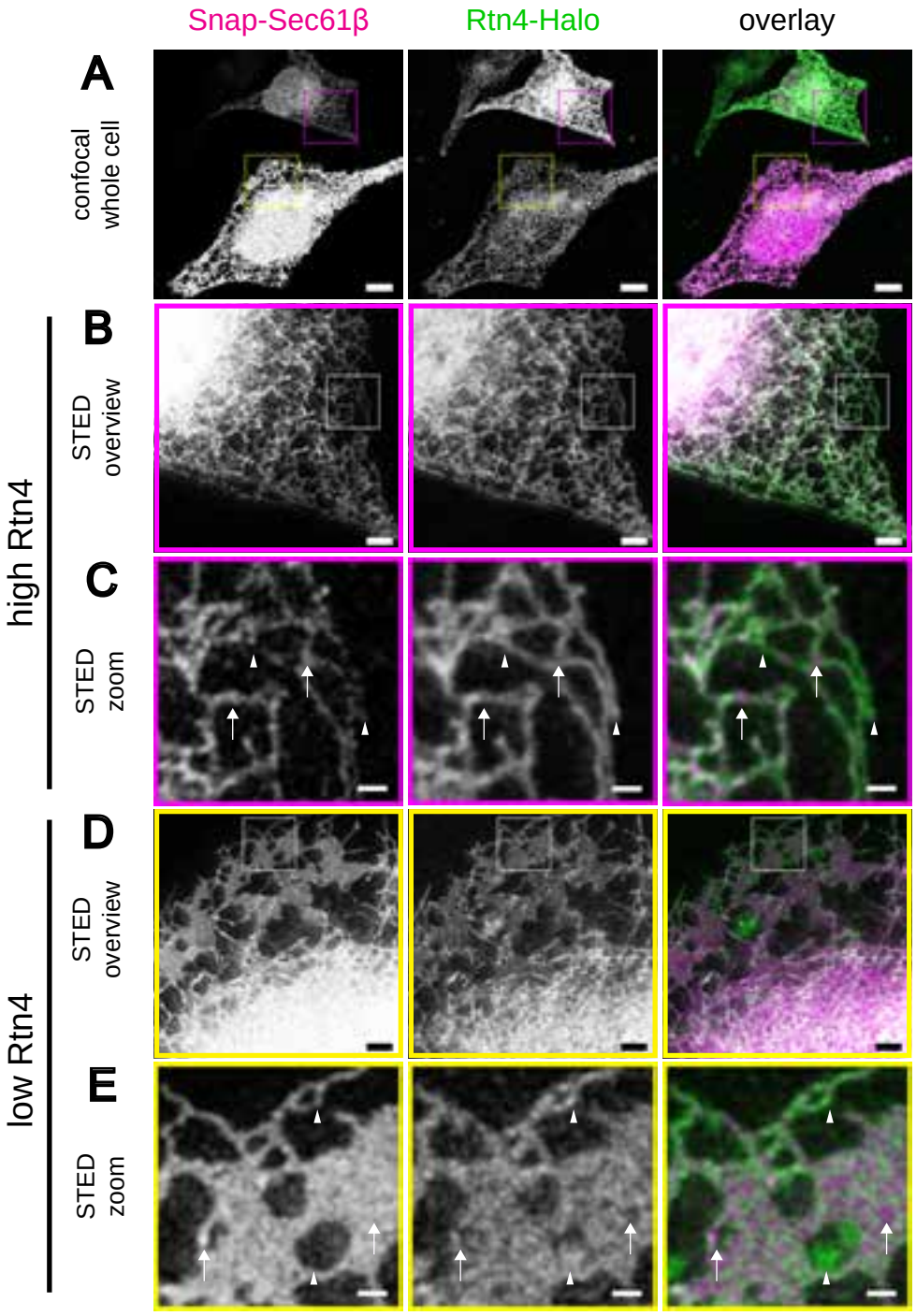

Figure 17: Different expression levels of Sec61β and Rtn4 in live-cells. SNAP-Sec61β and Rtn4-Halo were labeled with SiR-BG and A590-CA, respectively. (A) Confocal overview of cells with different expression levels. (B) STED overview of a cell region with high Rtn4 levels. (C) Magnification of boxed region in (B). Arrows show locations of high Sec61β levels and little Rtn4 signal. Arrowheads point at regions of high Rtn4 signal without Sec61β. (D) STED overview of a cell region with high Sec61β levels. (E) Magnification of boxed region in (D). Random localization of Rtn4 across sheet areas detectable. Left arrow points at localization of Sec61β on a tubule without Rtn4 signal. Right arrow points at one of the few Sec61β sheet areas without Rtn4. Upper arrowhead points at Rtn4 on a tubule region with almost complete exclusion of Sec61β. Lower arrowhead points at unspecific localization of Rtn4 in big ER hole. Scale bars (A) 10 µm, (B+D) 2 µm, (C+E) 0.5 µm.

3.7 High Rtn4 overexpression can reverse nocodazole effects

To induce ER sheet formation, Rtn4 overexpressing cells were subjected to nocodazole treatment. More specifically, SNAP-Sec61β and Rtn4-Halo co-overexpressing cells were labeled with SiR-BG and A590-CA, then treated for 30 min with 33 µM nocodazole, kept under nocodazole treatment on the microscope stage and imaged for up to one hour. As a control, one sample was transfected with Sec61β alone. Nocodazole treatment of these cells created sheets that showed very few micro-fenestrations (Figure 18), compared to the fixed cells under nocodazole treatment, which showed highly fenestrated sheets (see Figure 14).

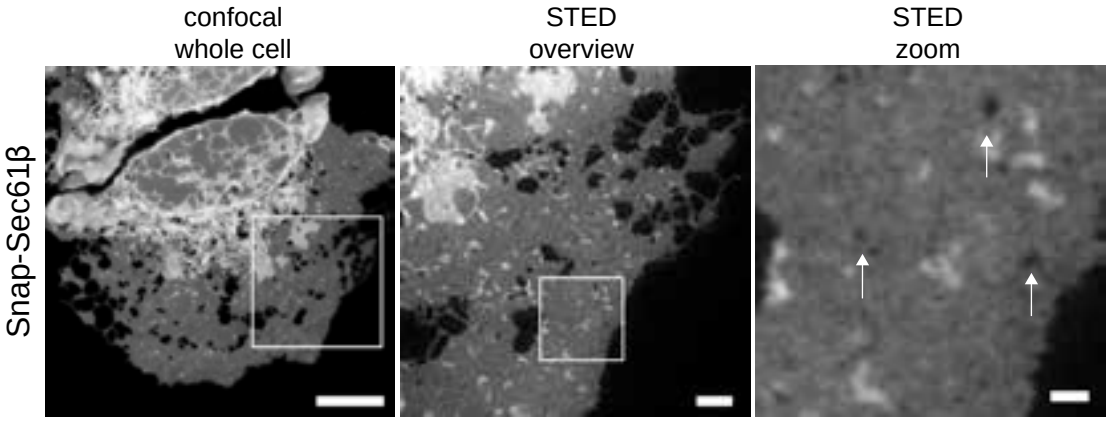

Figure 18: live-cell STED images of the ER under nocodazole treatment. The overexpressed ER marker SNAP-Sec61β was live-labeled with SiR-BG, cells were subjected to 33 µM nocodazole treatment for 30min and kept under treatment on the microscope for up to one hour. Typical cell morphology is shown on the left, one ROI was picked and a zoom-in is shown on the right. Arrows indicate micro-fenestrations. Scale bars: 10 µm, 2 µm and 0.5 µm

When the nocodazole treated cells were also overexpressing Rtn4, but at a low level (Figure 19), their ER consisted almost exclusively of sheets as expected. Rtn4 randomly localized across the whole sheet area without any specific pattern, comparable to their untreated counterpart (compare to Figure 17E).

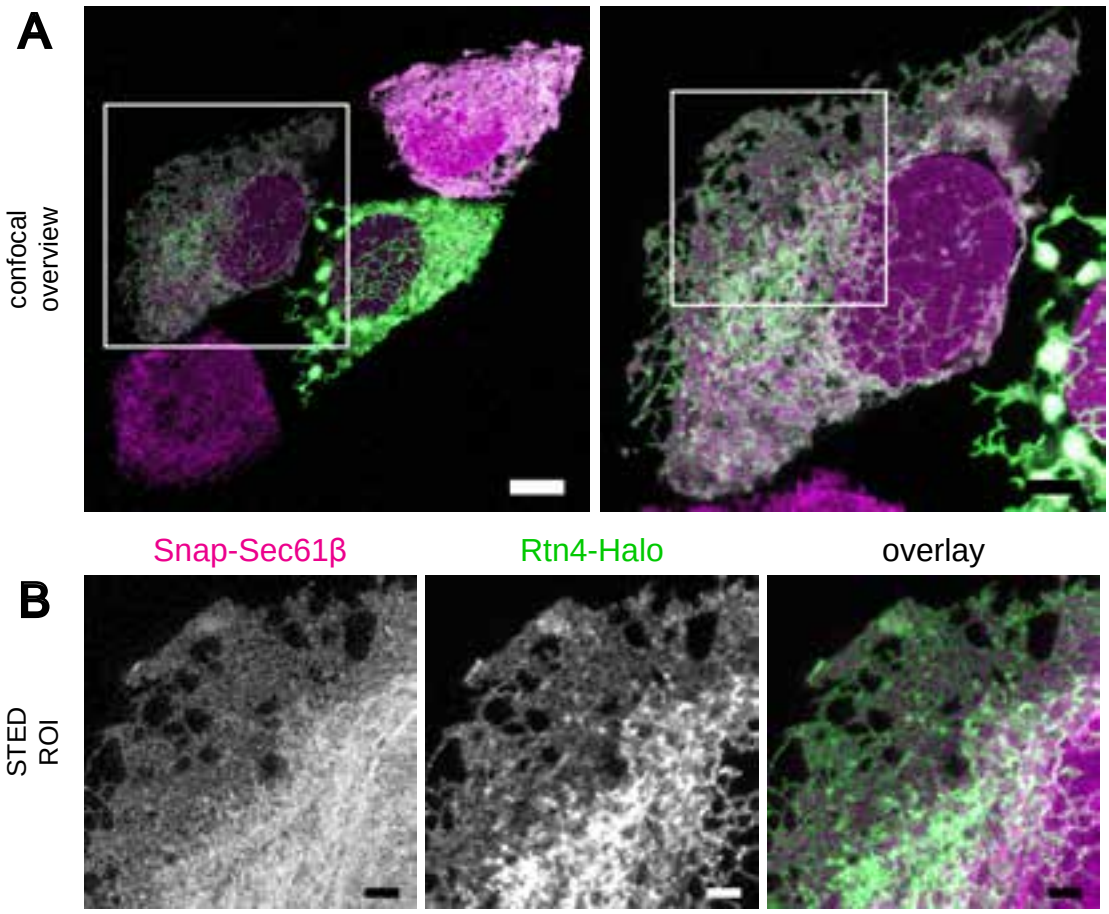

Figure 19: Live STED images of the ER and Rtn4 (low expression level) under nocodazole treatment. The overexpressed ER marker SNAP-Sec61β was live-labeled with SiR-BG, cells were subjected to 33 µM nocodazole treatment for 30min and kept under treatment on the microscope for up to one hour. (A) Overview of two neighboring cells with different expression levels, the cell with lower Rtn4 expression is shown on the right. (B) Magnification of the region boxed in the right panel in (A). Scale bars: (A) 10 and 5 µm, (B) 2 µm.

When the cells were highly overexpressing Rtn4, however, even after treatment with nocodazole, the ER still remained partially tubular (Figure 20). Here again, as already proposed by Voeltz et al. (2006) and described in Figure 16, some tubule areas seemed to be completely devoid of Sec61β, but had a very bright Rtn4 staining and other spots had a dim Rtn4 staining and Sec61β was more prominent (Figure 20C).

Consistent with Shibata et al. (2008), I not only found the ER to remain tubular after nocodazole treatment when Rtn4 was highly overexpressed, but I also saw bright Rtn4 foci on the ER (Figure 20B). Summarizing, these data suggest that overexpression of Rtn4 can counteract the effect of nocodazole treatment on the ER by stabilizing tubules. Rtn4 shows some alternating patterns with Sec61β but again, no specific localization of Rtn4 in micro-fenestrations could be determined. Furthermore the overexpression of Rtn4 created non-physiological ER morphologies.

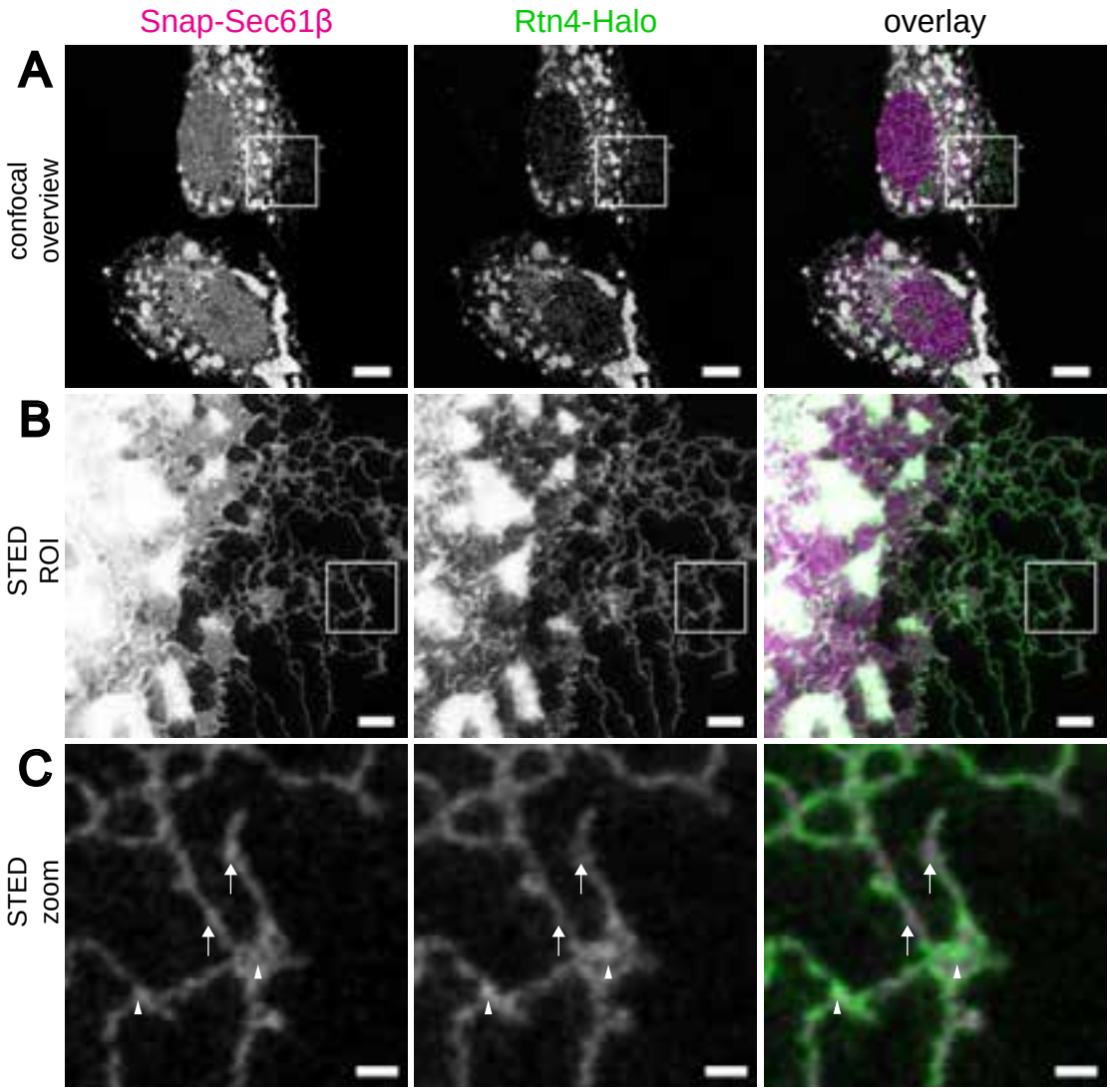

Figure 20: Live STED images of the ER and Rtn4 (high expression level) under nocodazole treatment. The overexpressed ER marker SNAP-Sec61β was live-labeled with SiR-BG, cells were subjected to 33 µM nocodazole treatment for 30min and kept under treatment on the microscope for up to one hour. (A) Overview of two neighboring cells with high Rtn4 expression levels. (B) Magnification of the region boxed in (A). (C) Zoom-ins of the boxed region in (B). Arrows show locations of high Sec61β levels and little Rtn4 signal. Arrowheads point at regions of high Rtn4 signal without Sec61β. Scale bars: (A) 10 µm, (B) 2 µm, (C) 0.5 µm.

3.8 Localization of endogenous Rtn4 needs to be determined in live-cells

To avoid the artificial situation created by protein overexpression and to investigate the localization of endogenous Rtn4 in living cells, I created a CRISPR cell line, in which Rtn4 is expressed with a C-terminal SNAP-tag (see Supplementary Figure S2A; also see Section 5.5). After antibiotic selection, the cells were sorted by flow-cytometry (see Supplementary Figure S2B) and only the brightest 30% were selected. These bulk sorted cells were used for preliminary experiments and frozen down as back-ups, as well as singularized to grow up clonal populations.

To ensure the functionality of Rtn4 in the CRISPRed cells, I investigated if the endogenous signal of Rtn4-SNAP was overlapping with the signal for Rtn4 detected by antibody staining. To this end, I labeled a set of bulk-sorted (non clonal but FACSed) CRISPR cells with SiR-BG (for the endogenous SNAP-tagged Rtn4), fixed them and stained for Rtn4 by indirect immunofluorescence.

Indeed, the Rtn4-SNAP and Rtn4-antibody stainings overlapped perfectly (Figure 21B). Some cells in this bulk sorted population seemed to carry some defective version of Rtn4-SNAP, because the protein localized randomly throughout the cytoplasm. Nonetheless, these cells showed a nicely localized Rtn4 antibody staining (see Figure 21A), which indicated that the two stainings were independent of each other. Therefore, I could exclude the possibility that overlapping signals were an artifact. One of the cells with perfectly overlapping stainings (Figure 21B) was magnified and again, the cells show the previously described discontinuous pattern of Rtn4 staining (Figure 21C). The Pearson coefficient for one representative tubule was 0.9, which is almost perfectly correlated (Figure 21D). These preliminary data indicate that the Rtn4 tagging via CRISPR had worked and subsequent experiments could be performed with these cells.

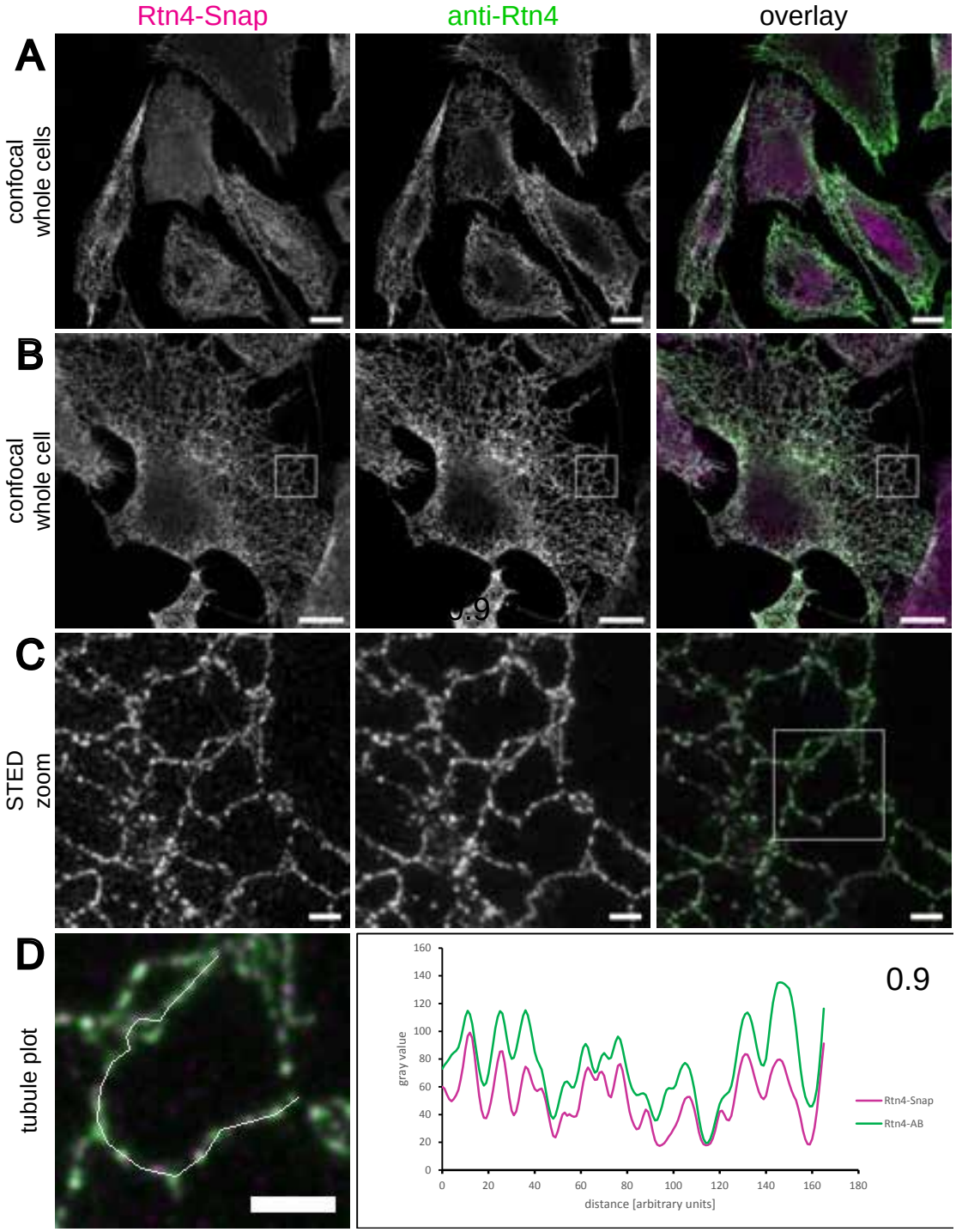

Figure 21: Endogenous Rtn4-SNAP (by CRISPR) co-localizes with Rtn4 antibody labeling. CRISPRed Rtn4-SNAP was live-labeled with SiR-BG. The antibody staining for endogenous Rtn4 was performed with a specific primary antibody and a secondary antibody coupled to the STED dye A594. (A) Overview of multiple cells, where some show a funky CRISPR staining, but an expected antibody staining. (B) Overview of a cell showing nice overlay of the two patterns. (C) Zooms of the boxed region in (B). (D) Zoom of the boxed region in (C). The tubule plot confirms co-localization. Pearson coefficient in the upper right corner. Scale bars (A-B) 10 µm, (C-D) 1 µm.

After the individual clones had grown up, I examined all of them for the expected staining pattern by live-cell imaging (Figure 22) and performed a PCR and western blot (WB) to confirm their genomic status. The positive clones of the PCR (Supplementary figure S2) and WB (Figure 23) perfectly confirmed the clones which showed the expected staining in the live-cell images. Altogether, out of 576 initial wells, 23 clonal cell populations grew up. Of these, only six were expressing Rtn4-SNAP and the three clones with the highest Rtn4-SNAP expression were chosen. All clones were heterozygous.

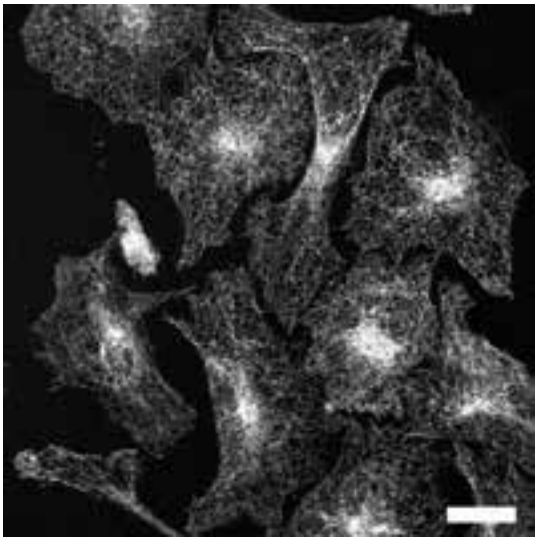

Figure 22: CRISPRed cells show expected reticular staining pattern of endogenous Rtn4-SNAP. Confocal live image of clonal cells carrying endogenous Rtn4 heterozygously tagged with SNAP. The cells were labeled with TMR-BG. Scale bar: 10 µm.

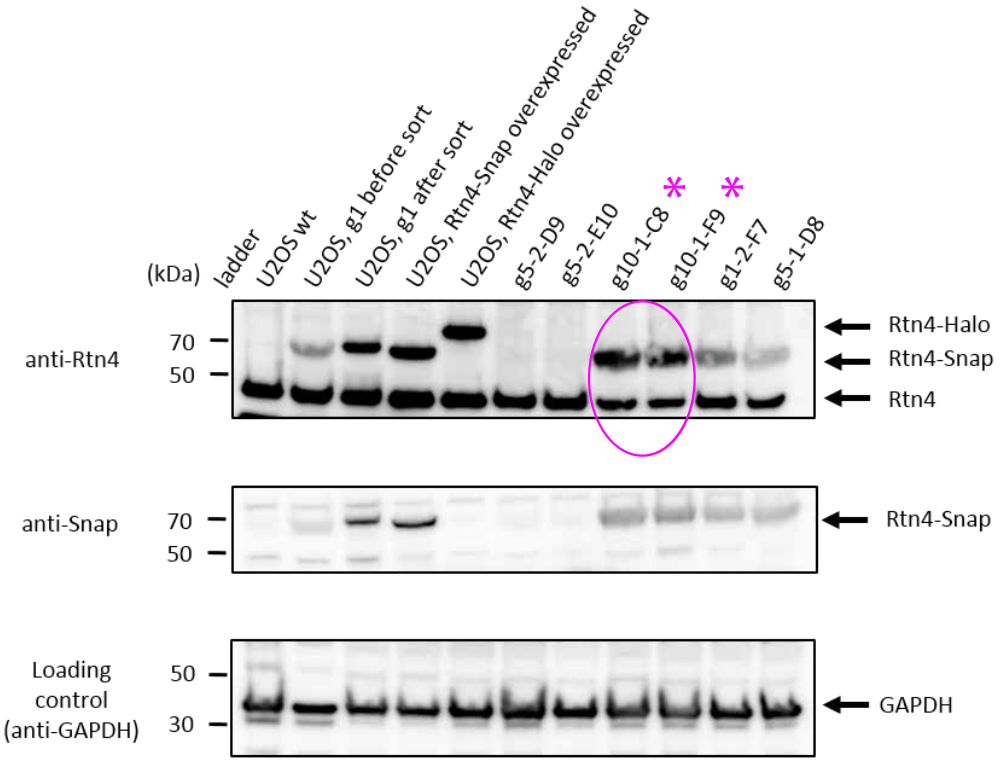

Figure 23: A western blot was performed with the single isolated CRISPR clones: two membranes were loaded with the same lysates, one was blotted for Rtn4 (detects a band of approximately 48 kDa, predicted molecular weight for Rtn4 isoform 2: 40 kDa), one was blotted for SNAP (20 kDa). Both were blotted for GAPDH (37 kDa). As loading controls were comparable for both membranes, only one is shown. Wt and 4 other controls to the left, 6 individual clones to the right. Favorite clones that carry the most Rtn4-SNAP on the protein level are marked with an asterisk. A second round of WB was performed with additional clones, and one more satisfying clone was found, but is not shown here.

One of the final clones was transfected with Halo-Sec61β and labeled with SiR-CA and A590-BG. However, because the protein was now endogenous and not overexpressed, the STED signal was so dim that the high background created by Atto590 was too high (data not shown). Therefore I had to switch to a different dye, TMR. Unfortunately this dye is not as easily depleted by STED and therefore does not give the same resolution improvement as Atto590. Still, the localization of the tagged Rtn4 could be perfectly observed on tubules in the ER (Figure 24) and the discontinuous pattern could be observed again. Also as previously shown, it depended highly on the expression levels of Sec61β whether there were a lot of sheets or not (Figure 24A (=low) vs B(=high)). No specific localization of Rtn4 could be found in micro-fenestrations by live imaging, but the signal was very dim and hazy and hard to analyze.

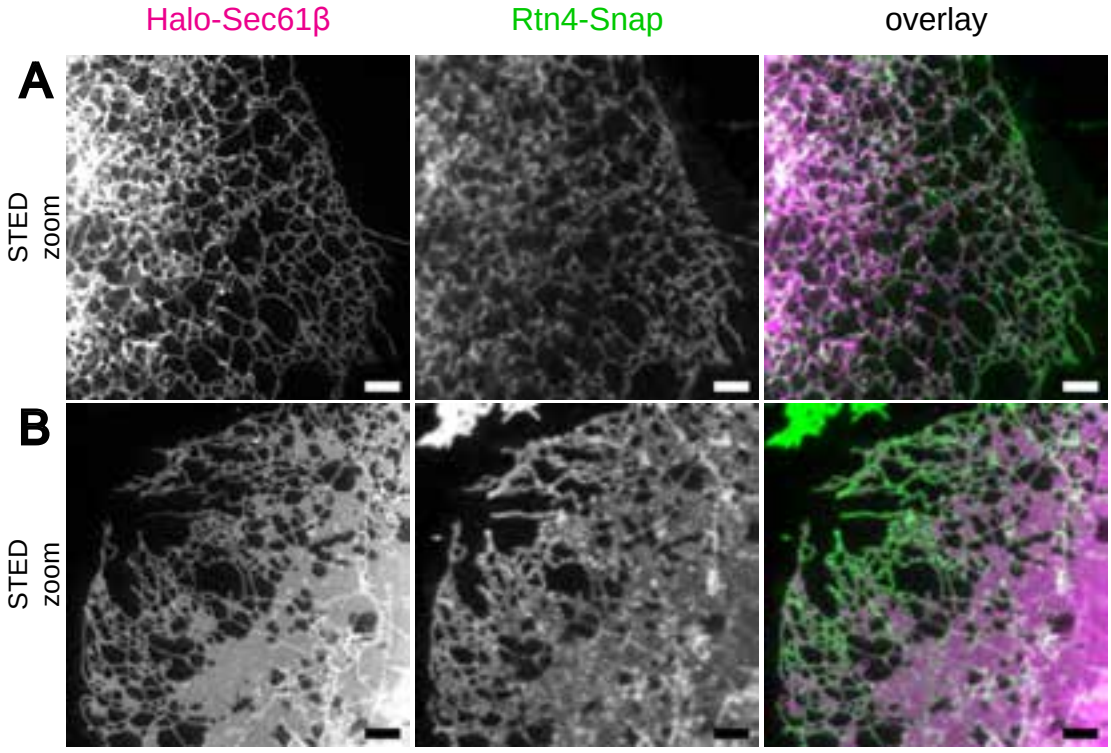

Figure 24: live-cell STED images of the overexpressed ER-marker Halo-Sec61β and endogenous Rtn4 (CRISPR). The overexpressed ER marker Halo-Sec61β was live labeled with SiR-CA. Rtn4-SNAP was visualized with TMR-BG. (A) Low level expression of Sec61β. (B) High level expression of Sec61β. Scale bars: 2 µm.

To increase the chances of obtaining higher quality images, the cells were fixed after labeling and then imaged (Figure 25). Although the acquisition of images is much easier in fixed cell samples due to the possibility of line and frame averaging, no Rtn4 could be found in the sheets but again the tubules showed the typical discontinuous pattern.

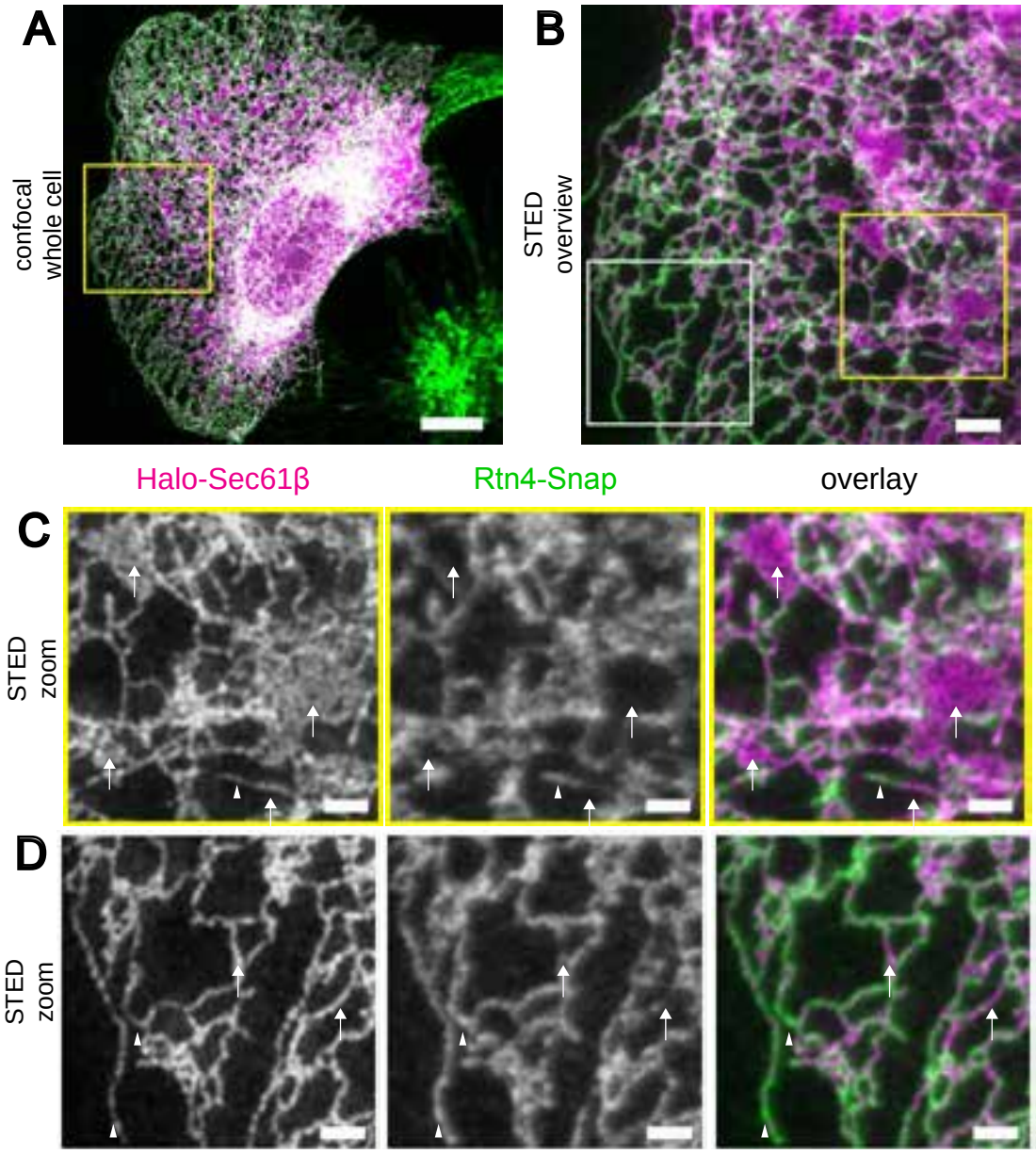

Figure 25: Fixed cell STED images of the overexpressed ER-marker Halo-Sec61β and endogenous Rtn4 (CRISPR). The overexpressed ER marker Halo-Sec61β was live labeled with SiR-CA and Rtn4-SNAP was labeled with TMR-BG. (A) Overview of the cell. (B) Magnification of the boxed region in (A). Overview of a region containing sheets and tubules. Rtn4 localizes beautifully to tubules and around sheet edges. (C) and (D) Zooms of the boxed regions in (B). Arrows show locations of high Sec61β levels and no Rtn4 signal. Arrowheads point at regions of high Rtn4 signal with low Sec61β staining. Scale bars: (A) 10 µm, (B) 2 µm, (C-D) 1 µm.

Together these data show that the CRISPR tagging had worked but due to various technical difficulties it will still take some optimization until we are able to get greater insights into the world of Rtn4.

4 Discussion and future outlook

By employing STED microscopy, we have shown that the ER of living cells consists of more complex sub-structures than just tubules and sheets. Micro-fenestrations, one type of these sub-structures, appeared surrounded by Rtn4 in fixed cell samples. When trying to reproduce this phenomenon in live-cells, the overexpression of Rtn4 created artifacts. Therefore I decided to endogenously tag Rtn4 via CRISPR, which was successfully employed. The resulting cell line is a valuable tool, which can be used to further investigate the localization of Rtn4 in live-cells.

Why does the ER contain different sub-structures? The different sub-structures and their intermediates point to the fact that the ER is multi-faceted and possibly even more dynamic than was thought before. The valuable insight I gained is only the first step to important knowledge about the organization, the biogenesis and the turn-over of these sub-structures and their functions. Their conservation suggests that they are functionally significant. Some of the sub-structures could be the precursors of others, they could have specific functions in different cell cycle stages or be more or less pronounced in different cell types. Importantly, the ER is continuous at all times, spreads out into every part of the cell and contacts almost every other organelle (English et al. (2009), Friedman and Voeltz (2011)). The result is a constant rearrangement, which is a very energy consuming process and must therefore happen for good reasons with very well adapted structures. Some of these structures - tubules for example, which feature high curvatures - are energetically unfavorable states. The ability to create and maintain these different structures also requires proteins. Therefore the interplay between structures and their molecular players needs to be understood in order to identify underlying functions.

What is the purpose of micro-fenestrations? Micro-fenestrations in ER sheets have been observed in fixed cells before (Palade (1956), Puhka (2011) Lieberman (1971)). As Puhka (2011) points out, the amount, shape and characteristics of micro-fenestrations vary a lot from cell type to cell type, which I can hereby confirm. This could indicate that micro-fenestrations have a defined function which might be more necessary in one cell type than the other, comparable to the fact that secretory cells, for example, have more ER sheets versus tubules. But what is the purpose of the micro-fenestrations? Lieberman (1971) for example saw microtubules passing through those holes in neuronal cells. This means they could be openings for other cellular components that would otherwise be blocked by an ER sheet. A different idea is that the micro-fenestrations are intermediates of tubules becoming sheets or

the other way around. Or maybe they are just the unwanted results of two opposing monolayers of ER that have collapsed and created a hole by periplasmic fusion, as was presented in the Golgi (Warren, 1995). In any case, insightful studies are missing and therefore it is important to thoroughly investigate the structures, especially now, that we can utilize those novel powerful tools of super-resolution light microscopy, which enable a new era of organelle research.

Why are micro-fenestrations different in size and abundance? In accordance with Puhka (2011), I could also detect the micro-fenestrations in ER sheets of nocodazole treated cells. Eventually, I found even more micro-fenestrations in nocodazole treated cells, than in untreated fixed or live-cells. However, controversially I could only see them when the nocodazole treated cells were fixed, whereas the ER sheets in nocodazole treated live-cells seemed to have very few micro-fenestrations. An attempt of an explanation for this could be as follows: Nocodazole treated live-cells seem to contain many micro-fenestrations which are so small that they are hard to resolve, even with STED. But why would the micro-fenestrations in nocodazole treated cells be smaller? The nocodazole-induced decrease in tubular surface forces all the curvature stabilizing proteins into sheet areas. In order to fit all of the curvature stabilizing proteins, the ER sheet needs to create abundant micro-fenestrations, which would therefore be smaller in order to fit more curvature-stabilizing proteins. Another hypothesis is that the micro-fenestrations in nocodazole treated cells move faster and are therefore harder to image, which could be solved with faster recording speeds. The fact that the holes seem to be bigger in fixed cells can result from the fact that the sample is not moving and therefore recording is much easier. The huge difference in micro-fenestration size of live vs fixed cells could, however, also result from a fixation artifact: Permeabilization does nothing else but perforating membranes, which means washing away lipids. Already existing holes that are too small to be seen in their natural state become enlarged through the permeabilization process which thereby seemingly creates micro-fenestrations, that are actually only getting bigger. Because of this and many more uncontrollable artifacts, live imaging is extremely important. However, achieving fast imaging is crucial. A very useful approach would be correlative live and then fixed cell imaging.

Is Rtn4 lining micro-fenestrations? The fact that overexpressed Rtn4 appears to be randomly localized over the sheet areas in live-cells could also be a result of the fact that it actually localizes to micro-fenestrations that are just too small to be seen. On the other hand, they could also just move too fast to be recorded. So far, I could detect the localization around micro-fenestrations only in fixed cells with an

antibody staining. Therefore, it remains to be elucidated by more advanced imaging, whether this was an artifact or is of actual biological relevance. It is, however, very intriguing that sheets and tubules have roughly the same diameter, which makes it seem likely that the same proteins account for the spacing. Hence, Rtn4 could shape tubules as well as induce the curvature at the edges of sheets and micro-fenestrations. Most micro-fenestrations in the fixed cell sample don't show a perfect ring surrounding them but a discontinuous pattern of Rtn4; sometimes even only two dots somewhere along the micro-fenestration edge. This could again be due to the aforementioned impairments of an antibody staining or more likely due to the fact that not every micro-fenestration has a continuous lining of Rtn4. As Shibata et al. (2008) state, reticulons don't need to cover the whole surface of a tubule in order to induce its shape. The same could be true for the micro-fenestrations. On the other hand, because the reticulons are so abundant and redundant (Voeltz et al. (2006)) and known to hetero-oligomerize (Shibata et al., 2008), Rtn4 might share the space with other reticulons, that are not detected by the Rtn4 antibody.

A hypothesis by Puhka (2011) was that fenestrated sheets could facilitate tubule formation out of sheets which she immediately dismissed as unlikely due to the fact that fenestrated sheets can be found at any given moment. The fact that Rtn4 could probably be located in those micro-fenestrations, however, makes this hypothesis seem more likely again. Maybe the reticulons specifically localize to the micro-fenestrations in order to form a new tubule out of the ER sheet, acting as a catalyst. Following this, reticulons are probably not inducing micro-fenestrations, but are only recruited to them at a later time point. When closely looking at the untreated fixed cell sample, one could faintly discern many minuscule holes, but they are not outlined by Rtn4. Potentially Rtn4 can only occupy a micro-fenestration after it has reached a certain size. It is also tempting to speculate that the localization depends on the stage of the cell cycle, as Anderson and Hetzer (2008) state that reticulons are needed for NE reformation after mitosis.

A discontinuous pattern of Rtn4 on tubules could be observed in fixed and live-cells. In the CRISPR cell line I could even show a perfect overlap of discontinuous antibody staining and discontinuous endogenous Rtn4. This makes it very likely that only partial rather than full coverage of the tubule's surface by Rtn4 is a biological phenomenon. This concurs with Shibata et al. (2008), who speculate that there are not enough reticulons in one cell to cover the whole surface of the ER tubules and sheet edges. Given the fact that there are more reticulons than just Rtn4 it makes even more sense that the Rtn4 staining is not continuous because Rtn4 might have oligomerized with some other reticulons. Besides, there needs to be space left for all the other ER membrane proteins. Although Voeltz et al. (2006) state that Rtn4

displaces Sec61β from the peripheral ER, I could not detect a pronounced anti-correlation, but rather a random distribution of Rtn4 and Sec61β independent of each other.

In contrast to the overexpression experiments, where Rtn4 was present on sheet areas, in the CRISPR cell line it proved completely absent from the sheets. Could it be that the tag of the CRISPR cell line is to big for the protein to fit in the microfenestrations any more? We can definitely reproduce the discontinuous pattern on tubules, which means that the Rtn4 must have retained most of its functionality. However, I saw a difference between SNAP- and Halo-tags in the overexpression plasmids. SNAP did not lead to the expected pattern. Maybe a new CRISPR cell line with Halo-tag needs to be created to rule out that the problem is specifically because of the SNAP-tag. Could the fact that the CRISPR cell line is not homozygous have something to do with it? More functional tests and repeated experiments are needed. Bright structures are clearly advantageous for STED imaging, a homozygously tagged protein would therefore be great.

Which other cool experiments can be done? A further experiment and logical step would be to do a knockdown of reticulons (compare to Anderson and Hetzer (2008)) to see if the morphologies of ER tubules, ER sheets and their microfenestrations change on a nanoscale level. This would be particularly interesting because reticulons are also needed for NE reformation after mitosis. The reduction of reticulons through siRNAs contributes to a faster NE formation (Anderson and Hetzer, 2008). It is not known whether this acceleration is due to the fact that the mitotic ER is then more sheet-like, or because the tubules that contact chromatin can be converted faster into sheets, once the reticulons are gone. Follow-up experiments would be to investigate the relationship between reticulons and other ER shaping proteins. The depletion of the atlastins or overexpression of dominant-negative forms inhibits tubule interconnections for example (Hu et al., 2009)). What would then happen in a double knock-down of reticulon and atlastin? Generally, a more quantitative approach has to be taken for all the claims made so far. Maybe even automated processing and image analysis could be helpful to rule out subjective errors in image interpretations. A particularly interesting approach would be to investigate the ER and reticulons in organoids or even tissues, for example with two-photon excitation STED. In order to achieve this, we would have to find very bright dyes that are bright enough to image endogenously tagged genes.

In summary, I have found the phenomenon of Rtn4 localizing around microfenestrations in fixed cells, which I could not yet reproduce in live-cells. Neither over-

expression, nor endogenous tagging lead to the expected result. However, my work contributes to the first steps of understanding ER sub-structures and Rtn4 function. By successfully engineering a CRISRPR cell line I created a valuable tool for these tasks. Employing better staining techniques, faster imaging parameters, knock-out experiments and other molecular biology techniques, as well as more quantitative approaches will eventually lead to resolving the localization of Rtn4, which in turn could lead to a better understanding of some reticulon-associated diseases.

5 Materials & Methods

5.1 General methods

5.1.1 PCR

By default Phusion® High-Fidelity DNA Polymerase (NEB #M0530L) was used for PCR with the standard HF buffer. When encountering difficult conditions, GC buffer or adding 5% DMSO to the reaction mixture could be the solution. dNTPs were thawed on ice. Each reaction mixture was set up on ice in PCR tubes:
10 µL 5x Phusion HF buffer
1 µL 10 mM dNTPs
2.5 µL 10 µM forward primer
2.5 µL 10 µM reverse primer
1 µL DNA template
0.5 µL Phusion
(2.5 µL DMSO)
32.5 (- 2.5) µL molecular grade water
50 µL total

Samples were put into a thermocycler at the following setting:
98 °C - 30 sec
35x [98 °C - 10 sec; 50 to 70 °C (annealing temperature according to primers) - 20 sec; 72 °C - 30 sec to 2 min (elongation time according to template size and manufacturer's specifications (Phusion polymerase: 4kb/min))]
72 °C - 10 min;
4 °C - forever;

5.1.2 Agarose DNA gel

To roughly check DNA fragments for their presence, size and abundance, e.g. after PCR or cloning, an agarose gel was cast. To this end, agarose was weighed in, mixed with the required amount of 1x TAE buffer and heated in the microwave until no more particles could be seen in the liquid. Agarose content was ranging between 0,8 up to 2 % of agarose (w/v), depending on the size of the expected product (the smaller, the more agarose). Usually the gel sizes ranged from 50 mL to 300 mL. After heating, the liquid was cooled down under running water until it could be touched and SYBR® Safe DNA gel stain (invitrogen) was added 1:10.000. The vessel was turned to spread the ethidium bromide and the mixture was poured into

a gel tray which was temporarily sealed with tape. Combs with various slot sizes and numbers were inserted. After hardening, the combs were pulled out and the gel tray was put into a gel chamber filled with 1x TAE buffer. The samples, which had been mixed with 6x purple gel loading dye (NEB B7024S), could then be loaded into the slots, as well as a marker (usually 5 µL of diluted 2-Log DNA Ladder (NEB N3200L), working dilution: 20 µL ladder + 33 µL 6x loading dye + 147 µL water). After closing the lid, and plugging in the cables in the right sense, the gels were run between 20 min and 2h at 100 Volts.

5.1.3 PCR purification

To further process or analyze PCR products they had to be purified to get rid of excess dNTPs, ions and enzyme. The QIAquick® PCR Purification Kit (Cat No./ID: 28106) was used. The 50 µL of the PCR reaction were mixed with 5x the volume of buffer PB. 10 µL of 3 M sodium acetate were added if the mixture was orange (happened mostly when DMSO was used in PCR). From here exactlly like 5.1.4: The mixture was applied to a QIAquick column and centrifuged for 30 sec at full speed. The flowthrough was discarded and 750 µL of buffer PE were added, 30 sec full speed, discard flowthrough. The column was spun once more to remove residual buffer. It was then placed in a new Eppendorf tube, 30 µL of buffer EB were added to the center of the column, incubated for 1 min and spun for 1 min full speed to elute purified DNA.

5.1.4 Gel purification

If two DNA fragments had to be separated or a PCR reaction gave a high background smear, a gel purification was performed with the QIAquick® Gel Extraction Kit (Cat No./ID: 28706). The DNA fragments were excised as narrowly as possible from the gel under UV light and put into a fresh Eppendorf tube. It was weighed and per 100 mg of gel 100 µL of buffer QG were added. This was incubated at 65 ℃ for 3 min shaking. 1 volume of isopropanol was added. From here exactlly like 5.1.3: The mixture was applied to a QIAquick spin column and spun for 30 sec at full speed (repeated multiple times if volume exceeded 750 µL). The flowthrough was discarded and 750 µL of buffer PE were added, 30 sec full speed, discard flowthrough. The column was spun once more to remove residual buffer. It was then placed in a new Eppendorf tube, 30 µL of buffer EB were added to the center of the column, incubated for 1 min and spun for 1 min full speed to elute purified DNA.

5.1.5 Sequencing

DNA was sent in for sequencing to the Keck DNA Sequencing Facility of the Yale School of Medicine. The purified DNA was premixed with water and primer according to the guidelines. 500-600 ng ds plasmid DNA template or 10-20 ng template for every 200 bases of PCR fragment length. Chromatograms were visualized with SNAPGene®.

5.1.6 Western Blot

NuPAGE® MES SDS Running Buffer (20X) was diluted with diH_2O to prepare 1X running buffer for blotting. Protein gels (NuPAGE™ Novex™ 10% Bis-Tris Protein Gels, 1.0 mm, 12-well, Invitrogen™ NP0302) were placed in the tray, which was filled with running buffer. 10 µL of the denatured protein lysates were loaded and 5 µL of a ladder as well (PageRuler™ Plus Prestained Protein Ladder, 10 to 250 kDa, Thermo Scientific 26619) and the gel was run for 35 min at 200 V.

Meanwhile, a 10X stock of transfer buffer was prepared by mixing 250 mM Tris base and 1.9 M glycine in water. A 1X solution was prepared by diluting 100 mL of the 10X stock with 700 mL of water and 200 mL of MeOH. PBS-T was prepared by mixing 0.5 mL 20 % Tween-20 and 100 mL 10X PBS in 1 L of water. Filter papers and sponges were soaked in transfer buffer. Membranes (Immobilon-P Membrane, PVDF, 0.45 µm, 15 x 15 cm sheet, EMD millipore IPVH15150) were cut to the right size and then wetted in MeOH for ~ 15 sec, then transferred to milliQ water and then equilibrated in transfer buffer.

After the gels were done running, the sandwich was assembled (add from bottom to top without air bubbles: sponge, [filter paper, gel, membrane, filter paper, sponge]x2, sponge) and put into the tray, which was filled with buffer. To cool the outer space, it was filled with water and the sandwich was run on RT at 30 V for 1 hr. Block buffer was always prepared freshly by adding 5 % milk to PBS-T. The membrane was taken out, (Ponceau stain optional) and put in block o/n at 4 °C. The next day the primary AB was added in milk usually at a conc of 1:500-1:5000) and incubated o/n. A loading control such as mouse-anti-alpha-tubulin was usually included as well. On the third day the membrane was washed 3 x 5 min with PBS-T on RT shaking. Then the secondary AB was added in milk. Typically a secondary AB coupled to AF488 (eg. Goat anti-Rabbit IgG (H+L) Secondary Antibody, Alexa Fluor® 488 conjugate, ThermoFisher A-11034) was used at 1:2000 and incubated at RT for 1 hr shaking and shielded from light. Then the membrane was washed 3 x 5 min with PBS-T on RT shaking again. Amersham ECL Western Blotting Detection Reagent (GEhealthcare, Product code: RPN2106) was used according to manufac-

turer's specifications. Then the membrane was ready to image on an ImageQuant LAS 4000 system.

5.2 Bacterial work

5.2.1 *E. coli* Transformation

Homemade competent *E. coli* DH5alpha cells were thawed on ice without mechanical movement (pipetting, shaking, snipping). 100 µL of the thawed cells were carefully transferred to a SNAPcap tube. The transforming DNA (10 ng - 2 µg) was added without mixing and the cells were incubated on ice for at least 30 min. They were then heat shocked at 42 °C for 60 sec, and cooled on ice for 2 min. 250 µL of S.O.C. medium (invitrogen no. 15544-034) without antibiotic were added and the cells were incubated at 37 °C shaking at 200 rpm for 1 hour in the bacterial shaker. They were then transferred to a 1.5 mL tube and spun down in the tabletop centrifuge for 3 min at 5000 rcf. The supernatant was discarded and the cells were resuspended in the remaining few µLs of liquid. They were then plated on agar plates containing the appropriate antibiotic using a Trigalski spatula. The plates were incubated over night at 37 °C and colonies could be picked the next day. For further use, plates were kept in the fridge up to several months.

5.2.2 Miniprep

To quickly isolate small amounts of bacterial plasmids, the Promega Wizard® *Plus* SV Minipreps DNA Purification system was used. One colony of a bacterial plate was inocculated in 3 mL of antibiotic containing LB medium in a SNAP cap tube and incubated over night at 37 °C on a bacterial shaker at 200rpm. The next day (max 18h later), this bacterial over night culture was centrifuged at 3400 g for 10 min at 4 °C. The supernatant was discarded and the pellet was resuspended in 250 µL of Cell Resuspension Solution and transferred to an Eppendorf tube. 250 µL of Cell Lysis Solution were added and the tube was gently inverted 4-6 times. 10 µL of Alkaline Protease Solution were added, gently inverted 4-6 times and incubated at RT for 5 min. 350 µL of Neutralization Solution were added and mixed immediately by inverting 4-6 times again. All steps were performed without vortexing, otherwise the chromosomal DNA would break and contaminate the plasmid isolation. The mixture was then centrifuged in a table top centrifuge for 10 min at top speed to pellet the chromosomal DNA. The supernatant (containing the plasmid DNA) was applied to a Spin Column which was inserted into a Collection Tube and centrifuged for 60 seconds at RT at top speed. The flow-through was discarded and the column

was washed by adding 750 µL of Wash Solution (with Ethanol added), centrifugation and discarding of the flow-through. A second washing step was performed with 250 µL of Wash Solution (with Ethanol added). After discarding of the flow-through, an additional round of centrifugation was performed to remove all liquid from the column. To elute the plasmid DNA, the column was placed onto a new Eppendorf tube, 50 µL of Buffer EB (Qiagen) were added onto the middle of the column, it was incubated for 1 min and then centrifuged for 1 min to obtain the final product. DNA concentrations were then measured with the help of a spectrophotometer. 5 µL of the freshly obtained plasmid and 95 µL of water were mixed and measured against a blank (100 µL water). Absorbance at 230nm, 260nm, 280nm and 320nm were measured and 260/280 and 260/230 were given by the machine as well. Anticipated results are at around 0.3 µg/µL and a 260/280 higher than 1.8.

5.2.3 Maxiprep

To isolate large, pure, concentrated amounts of plasmid DNA, the QIAGEN® Plasmid Maxi Kit was used. One colony was inocculated into 3 mL LB plus appropriate antibiotics in the morning and let grow for ~ 8 hours. In the meantime 1000 mL Erlenmeyer flasks were prepared with 240 mL of diH_2O and 6 capsules of LB and autoclaved. After autoclaving the appropriated drug was added and then 100 µL of the prepared dayculture were inocculated. The flasks were put into a bacterial shaker at 200 rpm o/n at 37 °C. The following morning they were transferred to high-speed compatible tubes and spun down in a special rotor at 5000 g for 15 min at 4 °C and then frozen at -20 °C or used right away. The pellets were resuspended very well in 10 mL of buffer P1 (with RNase A at 4 °C). 10 mL of buffer P2 was added and inverted 4 times and let lyse at RT for 5 min. 10 mL of prechilled buffer P3 was added and inverted 4 times and incubated on ice for 20 min. The lysates were then centrifuged for 30 mins at 4 °C at 20000 g. A QIAGEN-tip was meanwhile equilibrated by adding 10 mL of buffer QBT and letting it flow through. After the lysates were centrifuged, their supernatant was applied to the column and let flow through. The column was washed 2x with 30 mL of buffer QC. The DNA was then eluted in 15 mL buffer QF. 10.5 mL of isopropanol were added to precipitate the DNA, inverted 3 times and centrifuged for 30 mins at 4 °C at 15000 g. The supernatant was decanted very (!) carefully to leave the tiny DNA pellet in the tube. It was washed with 5 mL of 70% ethanol by vortexing and spun again for 10 mins at 4 °C at 15000 g. The supernatant was decanted very (!) carefully again to leave the tiny DNA pellet in the tube and it was air dried o/n. The next day it was resuspended in 1 mL buffer EB and put on a shaker o/n at 4 °C. Anticipated results are at around

1 µg/µL and a 260/280 higher than 1.8.

5.2.4 Glyerol stocks

700 µL of happily growing E.coli liquid culture and 300 µL of 50% glycerol were mixed in cryo-vials and frozen at -80 °C.

5.3 Overexpression plasmids

SNAP-Sec61β and Halo-Sec61β were kindly received from Lena Schroeder. I cloned the four Rtn4 plasmids. All of them were made by introducing the cDNA of the gene into one of the two starting vectors (Figure 26):

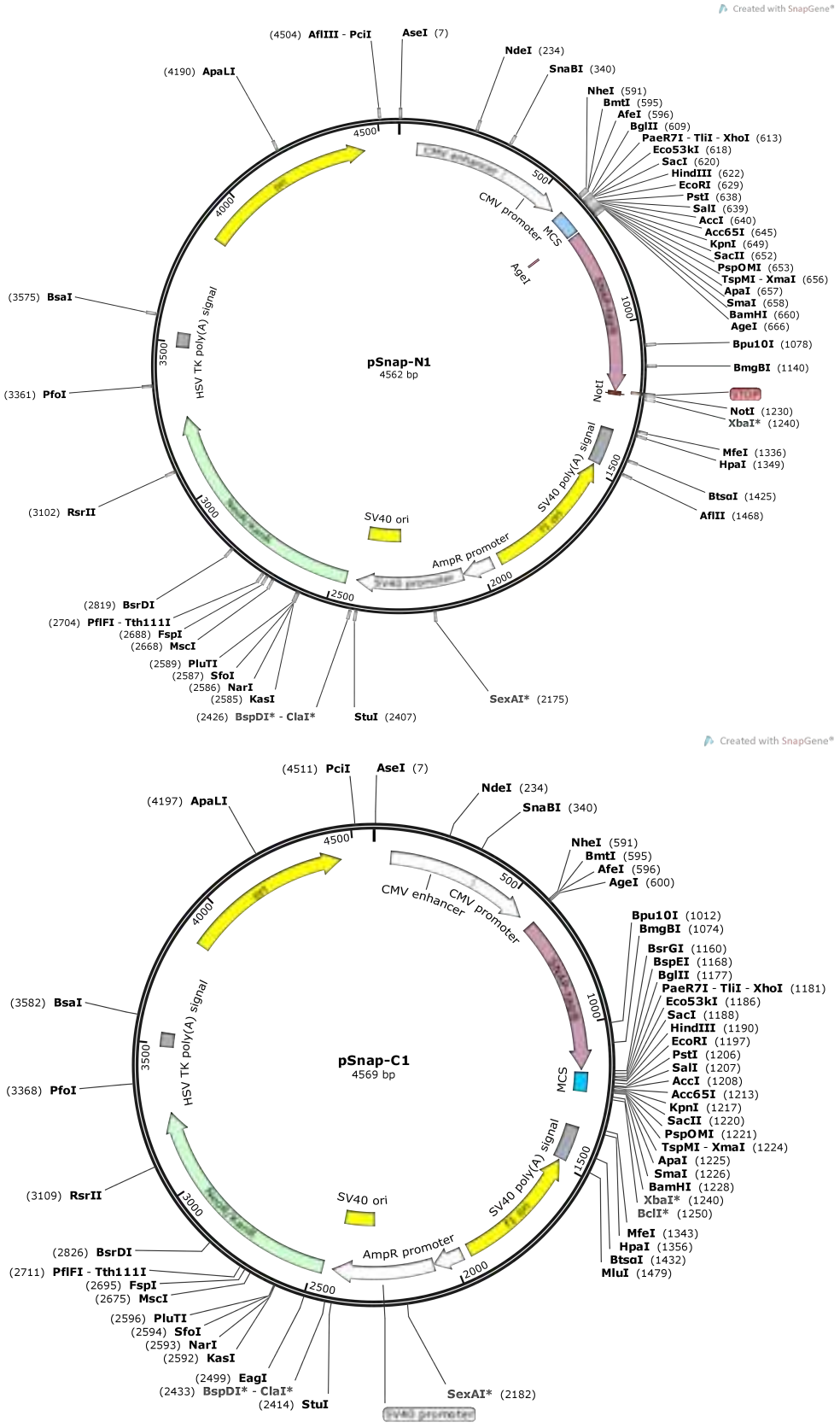

Figure 26: SNAP-tag vectors, which are identical to the respective Halo-tag versions, except for the tag of course.

5.4 Eukaryotic cell culture

5.4.1 Routine Cell Culture

U2OS cells were ordered from ATCC (ATCC® HTB-96™) and cultured in McCoy's 5A medium with 10% FBS (Gibco or Sigma) as recommended. They were split every 2-5 days by trysinisation up to a 1:20 dilution and discarded upon reaching p20. Cells were frozen at a concentration of $\sim 1 \times 10^6$ cells/mL in Cell Culture Freezing Media (Millipore #S-002-F). Mycoplasma tests were performed according to manufacturer's instructions with MycoAlert™ Mycoplasma Detection Kit (Lonza # LT07-118).

5.4.2 Transfection of eukaryotic cells

Electroporation Electroporation of eukaryotic cells was performed with the Nepa Gene Super Electroporator Nepa21 Type II. The trypsinized cells were washed 2 times with optiMEM (Gibco 31985-070) and adjusted to 1×10^6 cells/90 µL. These 90 µL were transferred to an electroporation cuvette (Bulldog Bio 12358-346). 10 µL of the DNA of interest were added (ideally 1 µg/µL = a maxiprep). This mixture was put into the electroporator and the according program was applied, after checking the current. The electroporated cells were then washed out into a 6-well plate by applying 500 µL of fresh medium 4 times to the cuvette.

Lipofection When high transfection efficiencies or cell survival mattered or generally with more tricky transfections of eukaryotic cells, lipofection was preferred over electroporation. The Lipofectamine® 2000 Reagent was used for this purpose. In two separate tubes the reaction was prepared. One contained 125 µL of optiMEM and 2.5 µg of DNA. The other contained 125 µL of optiMEM and 4 µL of Lipofectamine® 2000 Reagent. These two preparations were mixed together and incubated 5 min in order for the DNA-lipid complexes to form. 250 µL of the complexes were then added to 1 mL fresh media without antibiotics on cells that were ~ 75 % confluent. No media change was immediately required, but was performed the next day most of the time.

5.4.3 Nocodazole treatment

Cells were seeded at an appropriate confluence on #1.5 18 mm coverglasses. They might have been transfected or wildtype. On one of the following days (usually at ~ 50% confluence) they were covered with 250-300 µL of 33 µM nocodazole (6.6 mM stock in DMSO) in medium. They were incubated for exactly 30 mins at 37 °C. They

were then either kept under nocodazole treatment with the same concentration for up to one hour on the microscope stage. Or they were rinsed once quickly with PBS and fixed (see section 5.6.2).

5.4.4 Eukaryotic DNA isolation

DNA was isolated of eukaryotic cells with the QuickExtract™ DNA Extraction Solution from epicentre (QE09050). A confluent T75 or 10 cm dish was harvested by trypsinization, spun down and the pellet thoroughly resuspended in 500 µL of the extraction solution. It was then vortexed for 15 sec and transferred to 65 ℃ for 6 min. It was vortexed again and transferred to 98 ℃ for 2 min. The DNA could then be used right away (probably needed to be diluted 1:10 or so) or frozen at -20 ℃.

5.4.5 Protein lysates

900 µL of 4x Laemmli Sample Buffer (Biorad #1610747) were mixed with 100 µL of beta-mercaptoethanol. 100 µL of this were dispensed onto a confluent 6-well plate well and the cells were harvested in this buffer with a cell scraper. After transferring the lysates into an Eppendorf tube they could be stored at -80 ℃. Before use they were heated at 90 ℃ for 5 min.

5.5 CRISPR cell line production

All in silico cloning was performed by using the software SNAPGene®.

Cas9 plasmid pX165 was ordered from Addgene (Plasmid #48137, deposited by Zhang Lab) and came as a bacterial stab. It was expanded in presence of Ampicillin and miniprepd (see5.2.2) in order to get the plasmid.

gRNAs In silico design of the gRNAs was performed with the help of the online tool http://crispr.mit.edu/. A 200bp region around the stop-codon of Rtn4 was submitted, which led to 18 gRNAs. 3 gRNAs in close proximity to the stop codon were chosen to increase the chances of having at least one hit. The gRNA sequences were inserted into a 445bp-construct and ordered from IDT as gBlocks.

TGTACAAAAAAGCAGGCTTTAAAGGAACCAATTCAGTCGACTGGATCCGGTACC
AAGGTCGGGCAGGAAGAGGGCCTATTTCCCATGATTCCTTCATATTTGCATATACG
ATACAAGGCTGTTAGAGAGATAATTAGAATTAATTTGACTGTAAACACAAAGATATTA

GTACAAAATACGTGACGTAGAAAGTAATAATTTCTTGGGTAGTTTGCAGTTTTAAAA
TTATGTTTTAAAATGGACTATCATATGCTTACCGTAACTTGAAAGTATTTCGATTTCTT
GGCTTTATATATCTTGTGGAAAGGACGAAACACC*G*NNNNNNNNNNNNNNNNNNG
TTTTAGAGCTAGAAATAGCAAGTTAAAATAAGGCTAGTCCGTTATCAACTTGAAAAAG
TGGCACCGAGTCGGTGCTTTTTTTCTAGACCCAGCTTTCTTGTACAAAGTTGGCAT
TA

This 455bp fragment bears all components necessary for gRNA expression, namely:
U6 promoter + target sequence + guide RNA scaffold + termination signal
19bp of the selected target sequence were incorporated into the DNA fragment as 5'-NNNNN NNNNN NNNNN NNNNN NGG-3'

Prashant Mali (Church Lab), Version: 01-14-2013
To increase the quantity of DNA, a PCR of the gRNA gBlocks was performed with primers consisting of the first and last 20bp of the 455bp-scaffold.

HDR template The HDR template for creating a genomic Rtn4-SNAP fusion protein was engineered by using pSNAP-N1 as a starting plasmid (used to C-terminally tag proteins, MCS in front of tag, see Figure 26). The vector was linearized in the MCS by restriction digest with NdeI and ApaI (NEB): 1 µg pSNAPN1, 0.5 µL ApaI (NEB), 2 µL 10X cutsmart, 20 µL in total. Incubation at 25 ℃ for 60 min. Then 0.5 µL of NdeI were added and incubation at 37 ℃ for another 60 min. In order to prevent religation, calf intestinal alkaline phosphatase (CIP) was added and incubation at 37 ℃ for another 60 min. The pieces were then loaded onto a gel and the linearized vector was gel purified.

A left homoly arm (LHA) of around 1000bp next to the genomic cut site had been designed and ordered as gBlock. The exonic region identical to the gRNA sequence was silently point-mutated in order to prevent repeated cutting by Cas9 after homology dependent repair. The homology arm also contained a linker which should be inserted between the gene and its tag. This linker was found on iGEM (`http://parts.igem.org/wiki/index.php/Part:BBa_K243006`) and modified to a shorter length (ggtggttctggtggtggttctggt). The linker decreased the chances of sterical hindrance between the protein and tag. This LHA also had 20bp overhangs on either side identical to the 3' vector ends that resulted from the previous cutting. These 20bp overhangs were necessary in order to perform Gibson assembly. Gibson assembly was performed with the Gibson Assembly® Master Mix (# E2611S)

from NEB:
50ng of vector (5 µL of a 10ng/ µL solution)
26ng of insert (2,6 µL as the gBlock was diluted to 10ng/µL)
10 µL Gibson assembly master mix
Total: 20 µL
15 mins 50 °C, then 4 °C forever.

Bacteria were transformed with this newly made plasmid and streaked out on a Kanamycin plate. If colonies could be grown successfully, an o/n liquid culture was prepared to be miniprep'd. The plasmids were then sent for sequencing. After confirmation, the vector was linearized again. This was done with BsaI (NEB): 1 µg pSNAPN1+LHA, 1 µL BsaI (NEB), 2 µL 10X cutsmart, 20 µL in total. Incubation at 37 °C for 60 min. In order to prevent re-ligation, calf intestinal alkaline phosphatase (CIP) was added and incubation at 37 °C for another 60 min. The pieces were then loaded onto a gel and the linearized vector was gel purified.

A right homology arm (RHA) of around 1000bp next to the genomic cut site had equally been designed and ordered as gBlock. The genomic sequence identical to the gRNA sequence was mutated in this non-coding region after the stop codon in order to prevent repeated cutting by Cas9 after homology dependent repair.

This RHA also had 20bp overhangs on either side identical to the 3' vector ends that resulted from the previous cutting. These 20bp overhangs were necessary in order to perform Gibson assembly. Gibson assembly was performed with the Gibson Assembly® Master Mix (# E2611S) from NEB:
50ng of vector (5 µL of a 10ng/ µL solution)
26ng of insert (2,6 µL as the gBlock was diluted to 10ng/µL)
10 µL Gibson assembly master mix
Total: 20 µL
15 mins 50 °C, then 4 °C forever.

Bacteria were transformed with this newly made plasmid and streaked out on a Kanamycin plate. If colonies could be grown successfully, an o/n liquid culture was prepared to be miniprep'd. The plasmids were then sent for sequencing. After confirmation, the ready-made HDR plasmid (Figure 27) could be used for transfection of eukaryotic cells.

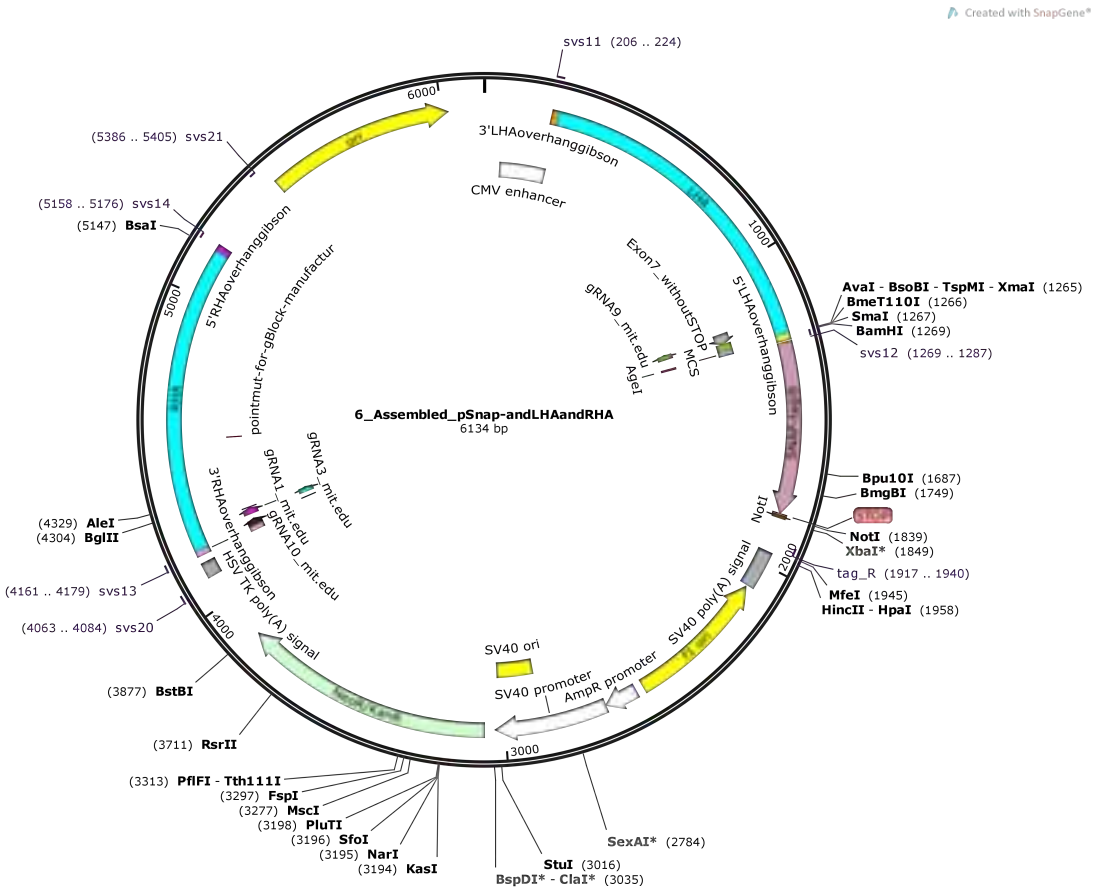

Figure 27: HDR template for Rtn4-SNAP

Workflow Eukaryotic cells were transfected with Lipofectamine. 3 µg of Cas9 plasmid, 3 µg of gRNA and 3 µg of HDR template were all transfected together into wt, low-passage mycoplasma free U2OS cells in 24-well plate wells. During the next days these cells were split into bigger vessels and a week after transfection, the selection with G418 (400 µg/mL) was started. After a week of selection, the cells were labeled with SiR-BG and sorted by flow cytometry. One cell per well was sorted into a 96-well plate and the rest was bulk sorted. The cells in the 96-well plate were incubated for over 3 weeks until clones would grow up. These were expanded and confirmed for the tagged gene by PCR and western blotting.

5.6 Imaging

5.6.1 Antibody-dye conjugation

87 µL of unlabeled secondary antibody (eg. donkey anti mouse) were mixed with 10 µL 1 M $NaHCO_3$ and 3 µL of 10 mM stock (in DMSO) of NHS (N-Hydroxysuccinimide) ester of the dye of interest. This mixture was incubated for 1 hr.

Size exclusion columns (GE healthcare illustra NAP-5 sephadex G-25) were installed over a beaker and the storage buffer was let flow out. The columns were primed by rinsing with three column volumes 1 x PBS. Then all of the above reaction was added until fully subsided into the column. A small amount of PBS was used to rinse. Two fractions would already become visible. More PBS was added until the first fraction eluted and could be caught in a tube (minus the first and last drop). The second fraction which is just unbound dye, was not collected. To calculate the number of dyes per antibody the absorption of the dye (specific) and the absorption of the antibody (280 nm) were measured on a spectrophotometer.

5.6.2 Immunofluorescence

Cells were seeded at an appropriate confluence on #1.5 18 mm coverglasses. On one of the following days (usually at ~ 50% confluence) they were carefully rinsed once with PBS and fixed with 3% PFA and 0.1% GA in PBS for 15 mins on a rocker at RT. The fixative was removed, the cells were rinsed 3x with PBS and the permeabilization buffer (0.3% NP40, 0.05% TritonX-100, 0.1% BSA in PBS) was applied for 3 mins rocking. Again 3x PBS rinse. Then the slides were immersed in block buffer (0.05% NP40, 0.05% TritonX-100, 5% donkey normal serum in PBS) and incubated at RT from 30 min up to several hours or even at 4 ℃ over night (usually 1 hour). The primary antibody was diluted in block buffer and applied directly without washes in between. Incubation times and temperatures were determined empirically:

goat anti Rtn4/NOGO (Santa Cruz, sc-11027) was diluted 1:500 and incubated over night at 4 ℃

mouse anti KDEL (Abcam ab12223) was diluted 1:500 and incubated over night at 4 ℃

After sufficient primary antibody incubation, the sample was washed 3x with wash buffer (0.05% NP40, 0.05% TritonX-100 and 0.2% BSA in PBS) for 5 min rocking. Then the secondary antibody was diluted in block buffer and applied to the sample rocking at RT for 1 hour.

donkey anti goat labeled with Atto594 (homemade dye conjugation) 1:200

goat anti mouse labeled with Atto647N was used 1:1000

After this secondary antibody incubation, the samples were again washed 3x for 5 min on rocker with wash buffer, then rinsed 3x with PBS and then mounted in ProLong® Diamond Antifade Mountant (ThermoFisher P36961) and let cure for at least 24h.

When a two- or more color staining was needed, the antibodies were added together, if the species specificities allowed, or successively.

5.6.3 Live-cell labeling

SiR-BG was obtained from NEB (SNAP-Cell® 647-SiR S9102S), SiR-CA was kindly distributed by Promega. A590-BG was made by Roman Erdmann (Schepartz lab) and A590-CA was made by Alex Thompson (also Schepartz lab). TMR-BG was obtained from NEB (SNAP-Cell® TMR-Star S9105).

Cells carrying either one or both of the tags (also see section 2.3) (either on an overexpression plasmid, on endogenously labeled genes via CRISPR or elsewhere) were seeded on KOH cleaned #1.5 18 mm coverglasses for later fixation, or in 8-well chambered Nunc™ Lab-Tek™ II Chambered Coverglass #1.5 (No° 155409) for live-cell imaging. When they reached reasonable confluence (~ 50 % confluent) or after at least 24-hour of expression, they were labeled by diluting the appropriate dye(s) to optimal concentrations (determinde empirically) and adding them to the sample for half an hour up to one hour.

The samples were then rinsed three times with room temperature PBS and a wash-out of the excess dye was performed by incubating another hour (up to three) with fresh medium. The cells were then ready for fixation or live imaging.

5.6.4 Microscope & imaging parameters

Imaging was performed on a Leica SP8 Gated STED 3X Super Resolution microscope in the Yale CCMI facility: It featured a 405 nm laser and a tunable (460 nm-660 nm) pulsed white light laser for excitation, three STED depletion lasers (592 nm (continuous wave), 660 nm (continuous wave), and 775 nm (pulsed), two PMT and two HyD detectors, temperature and CO_2 control-chamber and a 8000 Hz resonant scanner, all controlled by LAS-AX software suite. Images were taken using a 100x "STED white" high contrast plan apochromat (HC PL APO) oil objective with a 1.40 numerical aperture. Leica Type F Immersion liquid with a refractive index of 1.5180 was used. In order to comply with Nyquist, a pixel size no larger than 20 nm in STED mode was used. Usually a field size of around 50 x 50 - 100 x 100 µm was recorded for the confocal whole cell images and 19.38 x 19.38 µm (1024x1024 px) was the standard format for the ROIs. Zooms were usually cropped out of the ROI images. The pinhole was adjusted according to the longer wavelength to one airy unit. SiR and Atto647N were excited with 633 and 650 nm and the emission recorded between 650/660 nm - <720 nm. Atto590 and Atto594 were excited with 594 nm and emission recorded between 604 nm - 645 nm. STED confinement was only applied in 2D with STED laser powers varying widely from sample to sample from around 15 up to 100%. Fixed cells were usually imaged with the regular galvo scanner at 1000 Hz and averaged over four frames. Live-cells were mostly imaged

at 37 ℃ and 5% CO_2 with the 8000 Hz resonant scanner using up to 64 line averages. Live-cell imaging buffer was composed of 20 mM glucose in Live-Cell Imaging Solution (Molecular Probes® A14291DJ) (4.9 mL Solution + 100 µL 1 M glucose).

5.6.5 Image post-processing

Images have been contrast-adjusted with ImageJ. By adjusting the maximum slider to the left, the 256-bit gray scale range of an 8-bit image was re-distributed towards a smaller range in the brighter end of the spectrum, making all pixels appear brighter. A Gaussian blur was applied with a width of 2 pixels and overlays were prepared in ImageJ as well. Scale bars and boxes were added and subregions were cropped out in Adobe Photoshop. Final figures were prepared with Adobe Illustrator. Tubule profiles were plotted in ImageJ and values were transferred to Excel to make graphs and calculate the Pearson coefficient with the Excel built-in function.

6 Supplementary information

6.1 Rtn4 plasmids

Four different overexpression plasmids of Rtn4 were engineered (see section 5.2 and Figure S1A) and their localization was investigated through confocal microscopy (Figure S1B). The two Halo-tagged versions were considered functional and no difference between them could be observed (Figure S1B, left panels); they were hence used for further experiments. The linker length was defined by the remnants of the multiple cloning site and no additional linker fragments were introduced. The SNAP-tagged variants clearly did not lead to the expected reticular pattern (Figure S1B, right panels), which could be due to the short linker length and therefore some sterical hindrance of the protein function or other unknown reasons.

6.2 CRISPR confirmation

The Rtn4 tagged with SNAP by CRISPR was designed so that it has a linker (Figure S2A). Rtn4B (isoform2 on uniprot) was chosen, as it is widely expressed in cells except for liver. It has 373 AA and 40kDa (the antibody in western blot detects a band at around 48 kDa). After flow-cytometry (Figure S2B) and growing up of single clones, a western blot (23) and PCR (Figure S2C) were performed with the clones to obtain certainty about their tag insertion. The results from live-cell imaging were confirmed with all of the clones by PCR and WB. Clone g5-2-D9 for example looked like it had the signal uniformly blurred in the whole cytoplasm. By PCR

and WB, I could confirm that it had no DNA or protein of Rtn4-SNAP. Thankfully, three individual clones could be found that carried the tagged gene Rtn4-SNAP heterozygously at a decent expression level. These clones will be a very important tool for the further examination of endogenous Rtn4 function.

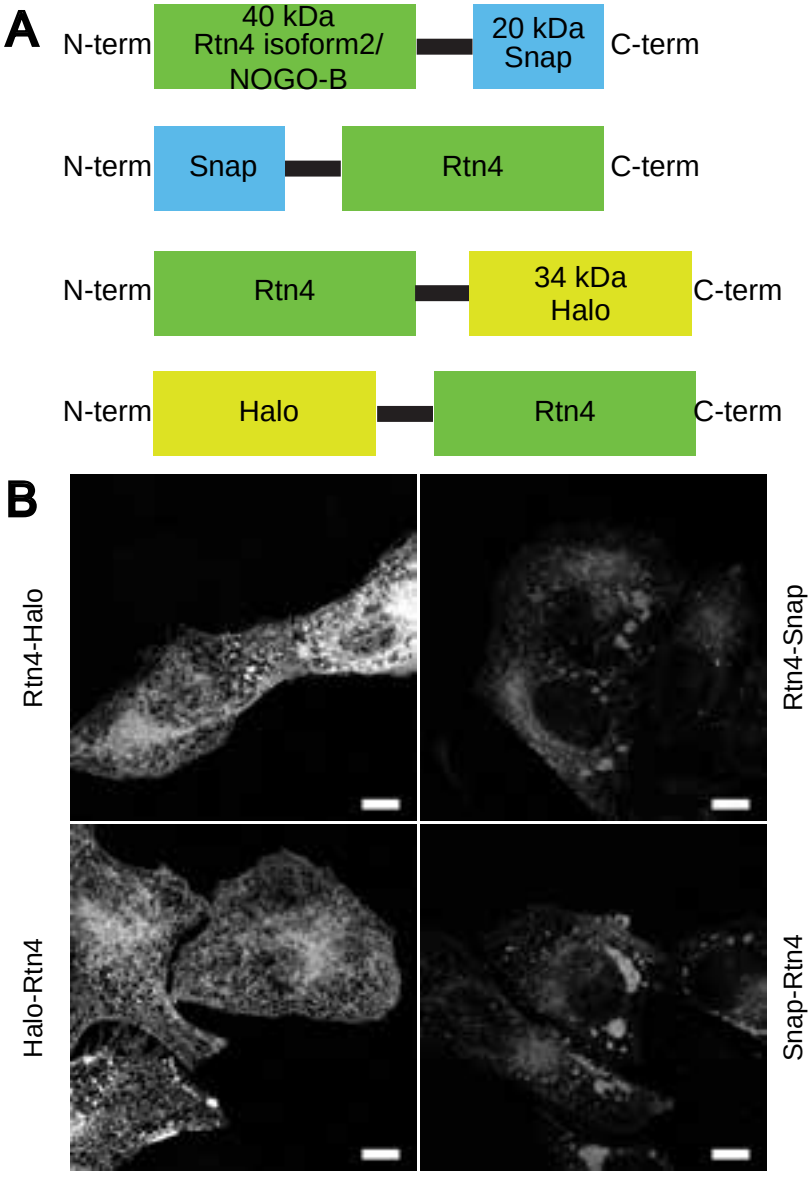

Figure S1: Rtn4 plasmids. (A) Schematics of the four different Rtn4 plasmids that were engineered. Rtn4 isoform 2 was chosen because it is expressed in all tissues except liver. (B) Confocal overview images of cells overexpressing the plasmids. Halo-versions on the left, SNAP-versions on the right. Scale bars: 10 µm.

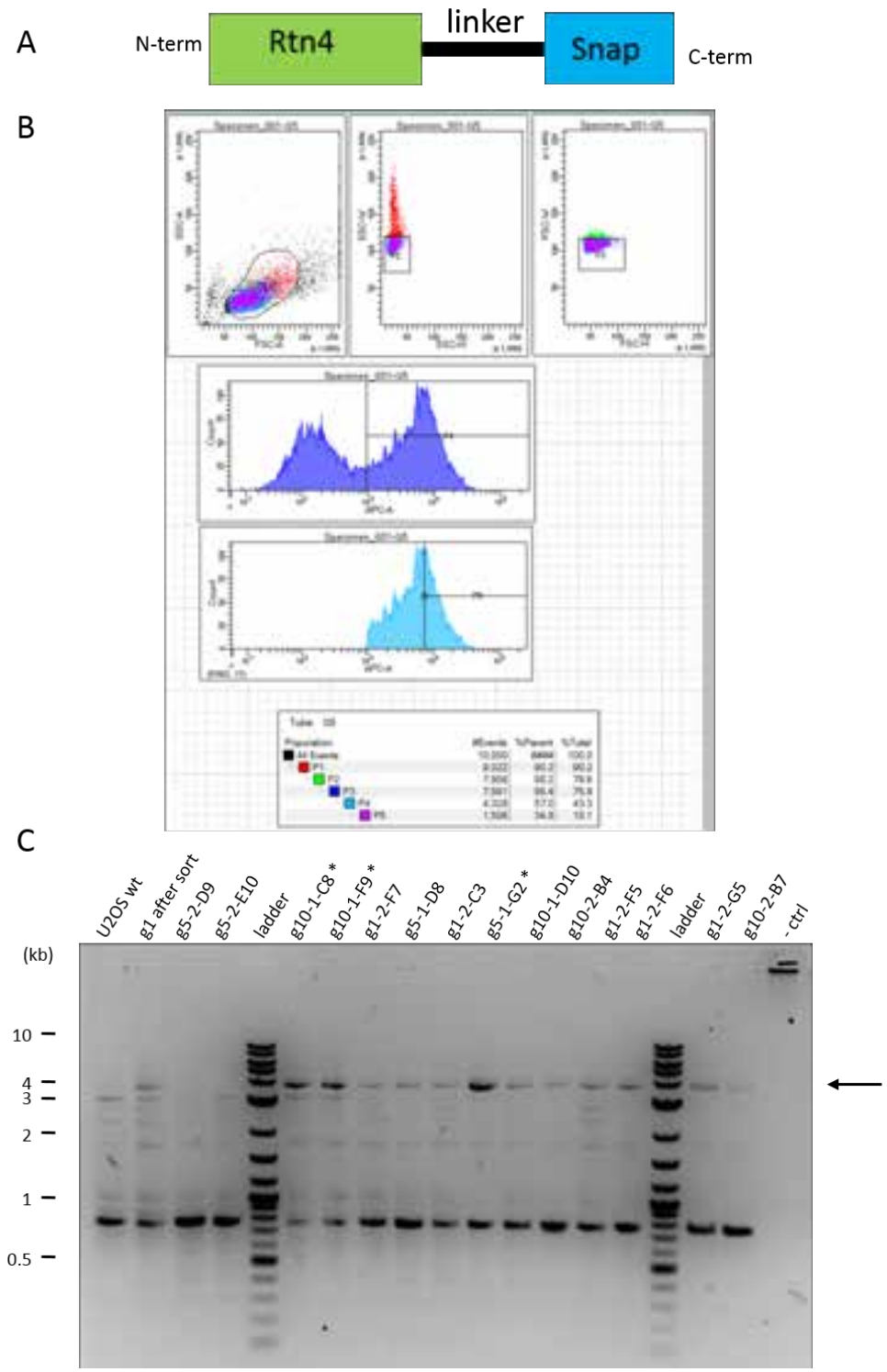

Figure S2: Construct, FACS and PCR. (A) The construct differs from the overexpression plasmid only by linker length. (B) FACS analysis: The cells were first gated for only living and to exclude duplettes. Then the fluorescent ones were chosen and of thos finally only the upper third. FACS blot representative for all three gRNAs. (C) PCR was performed with all clones with primers surrounding the insertion site. A 800bp wt piece and a 3700bp CRISPR piece were expected (marked by an arrow). Again, favorite clones were marked with an asterisk and correspond perfectly to the WB expression.

References

Abbe, E., 1873. Beiträge zur theorie des mikroskops und der mikroskopischen wahrnehmung. Archiv für Mikroskopische Anatomie 9 (1), 413–418.

Alberts, B., Wilson, J., Hunt, T., 2008. Molecular biology of the cell, 5th Edition. Garland Science, New York.

Anderson, D. J., Hetzer, M. W., 2008. Reshaping of the endoplasmic reticulum limits the rate for nuclear envelope formation. The Journal of cell biology 182 (5), 911–924.

Anzivino, G., Arnaudon, H., Baillon, P., Benetti, P., Boskma, L., Burger, P., Contin, A., DeSalvo, R., Gorodetzky, P., Grassi, D., Hao, W., He, H., Liu, L., Lundin, M., Mondardini, M., Paolucci, S., Rossella, M., Santiard, J., Schomaker, R., You, K., Wang, K., Wang, Y., Xia, X., Xu, C., Yang, C., Zhao, M., 1995. Review of the hybrid photo diode tube (hpd) an advanced light detector for physics. Nuclear Instruments and Methods in Physics Research Section A: Accelerators, Spectrometers, Detectors and Associated Equipment (365), 76–82.

Audhya, A., Desai, A., Oegema, K., 2007. A role for rab5 in structuring the endoplasmic reticulum. The Journal of cell biology 178 (1), 43–56.

Betzig, E., Patterson, G. H., Sougrat, R., Lindwasser, O. W., Olenych, S., Bonifacino, J. S., Davidson, M. W., Lippincott-Schwartz, J., Hess, H. F., 2006. Imaging intracellular fluorescent proteins at nanometer resolution. Science (New York, N.Y.) 313 (5793), 1642–1645.

Bottanelli, F., Kromann, E. B., Allgeyer, E. S., Erdmann, R. S., Wood Baguley, S., Sirinakis, G., Schepartz, A., Baddeley, D., Toomre, D. K., Rothman, J. E., Bewersdorf, J., 2016. Two-colour live-cell nanoscale imaging of intracellular targets. Nature communications 7, 10778.

Chen, M. S., Huber, A. B., van der Haar, M. E., Frank, M., Schnell, L., Spillmann, A. A., Christ, F., Schwab, M. E., 2000. Nogo-a is a myelin-associated neurite outgrowth inhibitor and an antigen for monoclonal antibody in-1. Nature 403 (6768), 434–439.

Di Scala, F., Dupuis, L., Gaiddon, C., de Tapia, M., Jokic, N., Gonzalez de Aguilar, J.-L., Raul, J.-S., Ludes, B., Loeffler, J.-P., 2005. Tissue specificity and regulation of the n-terminal diversity of reticulon 3. The Biochemical journal 385 (Pt 1), 125–134.

Ellenberg, J., Lippincott-Schwartz, J., 1999. Dynamics and mobility of nuclear envelope proteins in interphase and mitotic cells revealed by green fluorescent protein chimeras. Methods (San Diego, Calif.) 19 (3), 362–372.

Ellenberg, J., Siggia, E. D., Moreira, J. E., Smith, C. L., Presley, J. F., Worman, H. J., Lippincott-Schwartz, J., 1997. Nuclear membrane dynamics and reassembly in living cells: targeting of an inner nuclear membrane protein in interphase and mitosis. The Journal of cell biology 138 (6), 1193–1206.

English, A. R., Voeltz, G. K., 2013. Endoplasmic reticulum structure and interconnections with other organelles. Cold Spring Harbor perspectives in biology 5 (4), a013227.

English, A. R., Zurek, N., Voeltz, G. K., 2009. Peripheral er structure and function. Current opinion in cell biology 21 (4), 596–602.

Friedman, J. R., Voeltz, G. K., 2011. The er in 3d: a multifunctional dynamic membrane network. Trends in cell biology 21 (12), 709–717.

Friedman, J. R., Webster, B. M., Mastronarde, D. N., Verhey, K. J., Voeltz, G. K., 2010. Er sliding dynamics and er-mitochondrial contacts occur on acetylated microtubules. The Journal of cell biology 190 (3), 363–375.

Goyal, U., Blackstone, C., 2013. Untangling the web: mechanisms underlying er network formation. Biochimica et biophysica acta 1833 (11), 2492–2498.

GrandPre, T., Nakamura, F., Vartanian, T., Strittmatter, S. M., 2000. Identification of the nogo inhibitor of axon regeneration as a reticulon protein. Nature 403 (6768), 439–444.

He, W., Lu, Y., Qahwash, I., Hu, X.-Y., Chang, A., Yan, R., 2004. Reticulon family members modulate bace1 activity and amyloid-beta peptide generation. Nature medicine 10 (9), 959–965.

Hell, S. W., Wichmann, J., 1994. Breaking the diffraction resolution limit by stimulated emission: Stimulated-emission-depletion fluorescence microscopy. Optics Letters 19 (11), 780.

Hess, S. T., Girirajan, T. P. K., Mason, M. D., 2006. Ultra-high resolution imaging by fluorescence photoactivation localization microscopy. Biophysical journal 91 (11), 4258–4272.

Hu, J., Prinz, W. A., Rapoport, T. A., 2011. Weaving the web of er tubules. Cell 147 (6), 1226–1231.

Hu, J., Shibata, Y., Zhu, P.-P., Voss, C., Rismanchi, N., Prinz, W. A., Rapoport, T. A., Blackstone, C., 2009. A class of dynamin-like gtpases involved in the generation of the tubular er network. Cell 138 (3), 549–561.

Iwahashi, J., Hamada, N., Watanabe, H., 2007. Two hydrophobic segments of the rtn1 family determine the er localization and retention. Biochemical and biophysical research communications 355 (2), 508–512.

Keppler, A., Gendreizig, S., Gronemeyer, T., Pick, H., Vogel, H., Johnsson, K., 2003. A general method for the covalent labeling of fusion proteins with small molecules in vivo. Nature biotechnology 21 (1), 86–89.

Kohl, J., Ng, J., Cachero, S., Ciabatti, E., Dolan, M.-J., Sutcliffe, B., Tozer, A., Ruehle, S., Krueger, D., Frechter, S., Branco, T., Tripodi, M., Jefferis, G. S. X. E., 2014. Ultrafast tissue staining with chemical tags. Proceedings of the National Academy of Sciences of the United States of America 111 (36), E3805–14.

Lee, C., Chen, L. B., 1988. Dynamic behavior of endoplasmic reticulum in living cells. Cell 54 (1), 37–46.

Lieberman, A. R., 1971. Microtubule-associated smooth endoplasmic reticulum in the frog's brain. Z. Zellforsch. (Zeitschrift für Zellforschung und Mikroskopische Anatomie) 116 (4), 564–577.

Los, G. V., Encell, L. P., McDougall, M. G., Hartzell, D. D., Karassina, N., Zimprich, C., Wood, M. G., Learish, R., Ohana, R. F., Urh, M., Simpson, D., Mendez, J., Zimmerman, K., Otto, P., Vidugiris, G., Zhu, J., Darzins, A., Klaubert, D. H., Bulleit, R. F., Wood, K. V., 2008. Halotag: a novel protein labeling technology for cell imaging and protein analysis. ACS chemical biology 3 (6), 373–382.

Lukinavicius, G., Umezawa, K., Olivier, N., Honigmann, A., Yang, G., Plass, T., Mueller, V., Reymond, L., Correa, JR, I. R., Luo, Z.-G., Schultz, C., Lemke, E. A., Heppenstall, P., Eggeling, C., Manley, S., Johnsson, K., 2013. A near-infrared fluorophore for live-cell super-resolution microscopy of cellular proteins. Nature chemistry 5 (2), 132–139.

Oertle, T., Klinger, M., Stuermer, C. A. O., Schwab, M. E., 2003. A reticular rhapsody: phylogenic evolution and nomenclature of the rtn/nogo gene family. FASEB journal : official publication of the Federation of American Societies for Experimental Biology 17 (10), 1238–1247.

Palade, G. E., 1956. The endoplasmic reticulum. The Journal of Biophysical and Biochemical Cytology 2 (4), 85–98.

Prinjha, R., Moore, S. E., Vinson, M., Blake, S., Morrow, R., Christie, G., Michalovich, D., Simmons, D. L., Walsh, F. S., 2000. Inhibitor of neurite outgrowth in humans. Nature 403 (6768), 383–384.

Puhka, M., 2011. Morphogenesis of mammalian endoplasmic reticulum and golgi apparatus throughout the cell cycle. Ph.D. thesis, University of Helsinki, Helsinki.

Ran, F. A., Hsu, P. D., Wright, J., Agarwala, V., Scott, D. A., Zhang, F., 2013. Genome engineering using the crispr-cas9 system. Nature protocols 8 (11), 2281–2308.

Rust, M. J., Bates, M., Zhuang, X., 2006. Sub-diffraction-limit imaging by stochastic optical reconstruction microscopy (storm). Nature methods 3 (10), 793–795.

Shibata, Y., Voeltz, G. K., Rapoport, T. A., 2006. Rough sheets and smooth tubules. Cell 126 (3), 435–439.

Shibata, Y., Voss, C., Rist, J. M., Hu, J., Rapoport, T. A., Prinz, W. A., Voeltz, G. K., 2008. The reticulon and dp1/yop1p proteins form immobile oligomers in the tubular endoplasmic reticulum. The Journal of biological chemistry 283 (27), 18892–18904.

Terasaki, M., Chen, L. B., Fujiwara, K., 1986. Microtubules and the endoplasmic reticulum are highly interdependent structures. The Journal of cell biology 103 (4), 1557–1568.

Voeltz, G. K., Prinz, W. A., Shibata, Y., Rist, J. M., Rapoport, T. A., 2006. A class of membrane proteins shaping the tubular endoplasmic reticulum. Cell 124 (3), 573–586.

Vogel, S., Wainwright, S. A., 1969. A functional bestiary; Laboratory studies about living systems. Addison-Wesley series in life science. Addison-Wesley Pub. Co, Reading, Mass.

Warren, G., 1995. Intracellular membrane morphology. Philosophical transactions of the Royal Society of London. Series B, Biological sciences 349 (1329), 291–295.

Waterman-Storer, C. M., Salmon, E. D., 1998. Endoplasmic reticulum membrane tubules are distributed by microtubules in living cells using three distinct mechanisms. Current Biology 8 (14), 798–807.

Yang, Y. S., Strittmatter, S. M., 2007. The reticulons: a family of proteins with diverse functions. Genome biology 8 (12), 234.